

1 Date: May 11, 2020
2
3 Subject: Cover Letter for Revised Submission of bg-2019-508
4
5 Dear Reviewers and Associate Editor,
6
7 We thank you for taking time to read through our revisions. We have addressed all minor
8 comments as discussed below. Please find below our merged document containing Author
9 Responses and Changes (Page 2) and Tracked Changes starting on Page 3.
10
11 Best regards,
12
13 Dr Nicholas Parazoo (on behalf of all co-authors)
14 Jet Propulsion Laboratory
15 4800 Oak Grove Drive
16 Mail Stop 200-233
17 Pasadena, CA 91109
18 Phone: 818.354.2973
19

20 Comments and Author Response:

21

22 The authors have done a great job in replying to my comments and changing the manuscript
23 accordingly. Especially, the addition of SCOPE model simulations benefits the analysis a lot, I
24 find. I have just a few minor comments not requiring further reviewer assessment:

25

26 [We agree the addition of SCOPE was extremely beneficial, thank you for the suggestion](#)

27

28 I. 45: “distribution of light across sunlit and shaded leaves” or “within-canopy distribution of
29 direct and diffuse radiation”?!

30

31 [We changed to the former, thanks](#)

32

33 Fig. 1A: Replace “Climatology” in the legend

34

35 [Done](#)

36

37 I. 807: show instead of shows

38

39 [Done](#)

40

41 I. 887: “sunlit shaded fractions of leaf level” – what does that mean?

42

43 [This is poor wording – we really just mean emission of sif from sunlit and shaded fractions of
44 the leaf. We reworded the paragraph to clarify](#)

45

46

Wide Discrepancies in the Magnitude and Direction of Modelled SIF in Response to Light
Conditions

Nicholas C Parazoo¹, Troy Magney^{1,2}, Alex Norton³, Brett Raczka⁴, Cédric Bacour⁵, Fabienne
Maignan⁶, Ian Baker⁷, Yongguang Zhang⁸, Bo Qiu⁸, Mingjie Shi⁹, Natasha MacBean¹⁰, Dave R.
Bowling⁴, Sean P. Burns^{11,12}, Peter D. Blanken¹¹, Jochen Stutz⁹, Katja Grossman¹³, Christian
Frankenberg^{1,2}

Jet Propulsion Laboratory, California Institute of Technology¹

California Institute of Technology²

School of Earth Sciences, University of Melbourne³

School of Biological Sciences, University of Utah⁴

NOVELTIS, 153 rue du Lac, 31670 Labège, France⁵

Laboratoire des Sciences du Climat et de l'Environnement, LSCE/IPSL⁶

Colorado State University⁷

International Institute for Earth System Sciences, Nanjing University, China⁸

University of California Los Angeles⁹

Department of Geography, Indiana University¹⁰

Department of Geography, University of Colorado¹¹

National Center for Atmospheric Research¹²

Institute of Environmental Physics, University of Heidelberg¹³

Prepared for Biogeosciences

71 **Abstract:**

72 Recent successes in passive remote sensing of far-red solar induced chlorophyll fluorescence (SIF)
73 have spurred development and integration of canopy-level fluorescence models in global
74 terrestrial biosphere models (TBMs) for climate and carbon cycle research. The interaction of
75 fluorescence with photochemistry at the leaf- and canopy- scale provides opportunities to
76 diagnose and constrain model simulations of photosynthesis and related processes, through
77 direct comparison to and assimilation of tower, airborne, and satellite data. TBMs describe key
78 processes related to absorption of sunlight, leaf-level fluorescence emission, scattering and
79 reabsorption throughout the canopy. Here, we analyze simulations from an ensemble of process-
80 based TBM-SIF models (SiB3, SiB4, CLM4.5, CLM5.0, BETHY, ORCHIDEE, BEPS) and the SCOPE
81 canopy radiation and vegetation model at a subalpine evergreen needleleaf forest near Niwot
82 Ridge, Colorado. These models are forced with local meteorology and analyzed against tower-
83 based continuous far-red SIF and gross primary productivity (GPP) partitioned eddy covariance
84 data at diurnal and synoptic scales during the growing season (July-August 2017). Our primary
85 objective is to summarize the site-level state of the art in TBM-SIF modeling over a relatively short
86 time period (summer) when light, canopy structure, and pigments are similar, setting the stage
87 for regional- to global-scale analyses. We find that these models are generally well constrained
88 in simulating photosynthetic yield, but show strongly divergent patterns in the simulation of
89 absorbed photosynthetic active radiation (PAR), absolute GPP and fluorescence, quantum yields,
90 and light response at leaf and canopy scale. This study highlights the need for mechanistic
91 modeling of non-photochemical quenching in stressed and unstressed environments, and
92 improved representation of light absorption (APAR), distribution of light across sunlit and shaded
93 leaves, and radiative transfer from leaf to canopy scale.

Deleted: sunlit and shaded

97 **Section 1: Introduction**

98 Our ability to estimate and measure photosynthesis beyond the leaf scale is extremely limited.
99 This inhibits the ability to evaluate the performance of terrestrial biosphere models (TBMs) that
100 are designed to quantify the direct impact and feedbacks of the carbon cycle with climate change.
101 Consequently, there are substantial uncertainties in estimating the gross primary production
102 (GPP) response to environmental changes and carbon-climate feedback (Friedlingstein et al.,
103 2014). Global, multi-scale remote sensing of solar induced fluorescence (SIF) may represent a
104 major breakthrough in alleviating this deficiency (Mohammed et al, 2019). Spaceborne data
105 indicate a linear relationship between SIF and GPP at large spatial (kilometer) and temporal (bi-
106 weekly) scales (e.g., Sun et al., 2017) for several ecosystems, while theoretical models and
107 ground-based measurements indicate a more non-linear relationship at leaf and canopy scales
108 (Zhang et al., 2016; Gu et al., 2019; van der Tol et al., 2014; Magney et al., 2017, 2019a).

109 Chlorophyll fluorescence is re-emitted energy produced during the photosynthetic light
110 reactions, in which a small fraction (roughly 2%) of photosynthetic active radiation (PAR)
111 absorbed by chlorophyll is re-emitted at longer wavelengths (650-850 nm) as fluorescence. In
112 ambient conditions, the emission of SIF represents a by-product of two primary de-excitation
113 pathways, photochemical and nonphotochemical quenching (PQ, NPQ). Plants have evolved
114 these regulatory mechanisms to prevent damage to photosynthetic machinery when the amount
115 of absorbed radiation is greater than that which can be used to drive photochemistry. Chlorophyll
116 fluorescence responds dynamically to changes in photochemistry and NPQ from instantaneous
117 to hourly, daily, and seasonal timescales, as a function of changing environmental conditions and
118 plant structural properties (Porcar-Castell et al., 2014; Demmig-Adams et al., 2012). SIF is
119 fundamentally different than steady-state fluorescence yield typically measured at the leaf scale
120 as it is sensitive to both changes in photochemistry as well as absorbed PAR (APAR, related to
121 incident light, canopy structure, and biochemical content). The response of canopy SIF to APAR
122 is well documented in deciduous and evergreen forests and cropping ecosystems (Yang et al.,
123 2018; Badgley et al, 2017; Miao et al., 2018; Magney et al., 2019b; Li et al., 2020). More recently,
124 Magney et al. (2019b) showed that seasonal changes in canopy SIF for cold climate evergreen

125 systems is influenced by changes in needle physiology and photoprotective pigments (Magney et
126 al., 2019b).

127 To properly account for these factors, process-based SIF models must represent these underlying
128 non-linear biophysical and chemical processes. Several modeling groups have adapted TBMs to
129 incorporate various SIF formalisms for the purpose of model evaluation, data assimilation, and
130 improved model prediction (Lee et al., 2015; Koffi et al., 2015; Thum et al., 2017; Norton et al.,
131 2019; Bacour et al., 2019; Raczka et al., 2019). With these goals in mind, TBM SIF modeling
132 requires two important steps: (1) a representation of SIF at the leaf scale that accounts for NPQ
133 and photochemistry, and (2) canopy radiative transfer of SIF, which enables a comparison to large
134 field-of-view observations (e.g. tower, satellites). The second step involves accounting for
135 radiative transfer within the canopy and has typically relied on incorporating the Soil Canopy
136 Observation Photosynthesis Energy model (SCOPE, van der Tol et al., 2009, 2014), which
137 simulates chlorophyll fluorescence as a function of biophysics, canopy structure, environmental
138 conditions, and sun/sensor geometries. This approach has been adopted by TBMs in various ways
139 using different assumptions for fluorescence modeling and radiative transfer, as will be discussed
140 in Section 2.

141 Typically, measuring chlorophyll fluorescence and competing pathways (PQ, NPQ) has been done
142 at the leaf scale via pulse-amplitude modulation fluorescence (PAM, Schreiber et al., 1986).
143 Recently, commercially available spectrometers have made it possible to measure SIF directly in
144 the field at the leaf and canopy scale, and also enable the study of structural, environmental, and
145 directional controls (Cogliati et al. 2015; Daumard et al. 2010; Migliavacca et al. 2017; Yang et al.
146 2015; Grossman et al., 2018; Aasen et al., 2019; Gu et al., 2019b; Zhang et al., 2019). The use of
147 field deployable instruments on eddy covariance towers has increased rapidly since 2014,
148 providing coverage of multiple vegetation types across various climates around the world (Yang
149 et al., 2018; Magney et al., 2019a,b; Parazoo et al., 2019). These data enable improved
150 understanding of the relationship between SIF, GPP, APAR, and environmental effects at canopy
151 scales. Novel tower-mounted spectrometer systems such as Fluospec2 (Yang et al., 2018),
152 Photospec (Grossman et al., 2018), and FLOX (e.g., Julitta et al., 2017; Shan et al., 2019) have
153 made it possible to monitor canopy SIF continuously in the field with high precision over multiple

years providing opportunities for more direct comparison and evaluation of satellite data (Grossman et al., 2018; Yang et al., 2015, 2018; Wohlfahrt et al., 2018; Magney et al., 2019b). PhotoSpec offers the additional benefits (and challenge) of (a) precise field of view capable of resolving leaf-level SIF, and (b) canopy scanning at azimuth and elevation angles. These features enable SIF integration from leaf- to canopy- scales, and interpretation of directional variations of the emitted radiance.

Canopy scanning spectrometers such as PhotoSpec thus provide an opportunity to understand the physical processes that lead to a breakdown of SIF-GPP linearity at leaf to canopy scale (or conversely, emergence of linearity at increasing scale), and for detailed evaluation and diagnosis of TBM performance. This study provides a preliminary benchmarking site-level assessment for simulations of SIF within a TBM framework and across an ensemble of TBMs, with the primary purpose being an initial investigation into the response of modelled SIF and GPP to light during peak summer. We leverage continuous measurements of SIF and GPP at the Niwot Ridge US-NR1 Ameriflux flux tower in Colorado from June-July 2017 (Magney et al., 2019b), and simulations of canopy radiative transfer, photosynthesis, and fluorescence from a stand-alone version of SCOPE, to (1) Benchmark TBM-SIF modeling, (2) Evaluate sensitivity to underlying processes and scaling techniques, (3) Identify strengths and weaknesses in current modeling strategies, and (4) Recommend strategies for models and observations.

The paper is organized as follows: Section 2 describes SCOPE and the seven TBM-SIF models (SiB3, SiB4, ORCHIDEE, BEPS, BETHY, CLM4.5, CLM5) which have recently been published or are in review, and provides more details on site level benchmarking observations. Section 3 summarizes results comparing modelled and predicted SIF and GPP at hourly and daily scales, as they relate to absorbed light, GPP and SIF yields, and quantum yields. Section 4 discusses results in more detail, including attribution of SIF magnitude and temporal phasing biases and sensitivities to absorbed light, and areas for improvement.

Section 2: Methods

2.1 Site: Niwot Ridge, Colorado

Our study focuses on an AmeriFlux (<https://ameriflux.lbl.gov/>) site in Niwot Ridge, Colorado, USA (US-NR1), where a tower-based eddy covariance system has been continuously measuring the net ecosystem exchange of carbon dioxide (NEE) over a high-elevation subalpine forest since 1999, and a spectrometer system that has been continuously monitoring SIF since June 2017 (Grossman et al., 2018; Magney et al., 2019b). The 26 m tall tower is located in a high elevation forest (3050 m asl) located in the Rocky Mountains of Colorado (Burns et al., 2015; Hu et al., 2010; Monson et al., 2002) and consists primarily of the evergreen species of lodgepole pine (*Pinus contorta*), Engelmann spruce (*Picea engelmannii*), and subalpine fir (*Abies lasiocarpa*). The mean annual temperature is 1.5°C and mean annual precipitation is 800 mm (65% as snow). The forest is roughly 120 years old with a mean canopy height of 11.5 m, and a leaf area index of 4.2 m² m⁻². More site-specific details can be found in Burns et al. (2015).

At Niwot Ridge, interannual variations in GPP are closely linked to winter snowfall amount, which typically melts by early June, and summer precipitation, characterized by afternoon convective thunderstorms triggered by upslope flow (Burns et al., 2015; Albert et al., 2017) and climatological peak precipitation around 2 pm local time (Fig 1A). We note that our study period of July-August 2017 is unusual for NR1 (relative to the 2015-2018 mean) in its bimodal distribution of diurnal precipitation (morning and afternoon peaks), lower than normal afternoon precipitation, cooler temperatures, and reduced vapor pressure deficit (Fig 1 A-C). The early morning peak is due to a strong storm system that moved through from July 22-24 (Fig 1E), and does not show up when these days are removed. This period also shows a decrease in incoming shortwave relative to climatology despite lower precipitation (Fig 1D). We note that a second storm passed through in early August. The combination of these two storms produced net decreases in air temperature (Fig 1F), vapor pressure deficit (Fig 1G) and sunlight (Fig 1H) over a two-week period from late July to early August.

2.2 Tower-Based Measurements: PAR, SIF, CO₂ Flux

2.2.1 Absorbed PAR

The site is equipped with two main upward-facing PAR sensors. The first (LICOR LI-190R), mounted on the PhotoSpec telescope unit, provides an independent measurement of

direct/diffuse light and can be used to calibrate PhotoSpec (Grossman et al., 2018). The second (SQ-500-SS; Apogee Instruments), mounted on the main flux tower, is part of a larger array of upward- and downward-oriented PAR sensors above and below the canopy used for the calculation of the fraction of PAR absorbed by the vegetation canopy (fAPAR). The two PAR sensors show a similar diurnal pattern during July-August 2017 (Fig S1), including an afternoon dip and relatively smaller values overall compared to 2018 (the only other year with available PAR for comparison).

Full-spectrum quantum sensors (SQ-500-SS; Apogee Instruments) were new and factory-calibrated together just before installation. Above-canopy sensors (one up and one down-facing) were mounted on the main flux tower, and below-canopy sensors (six up and six down) were mounted at the 2 m height above ground on a shorter canopy-access towers. APAR was calculated for each pair of below-canopy relative to above-canopy sensors for every half-hour, then averaged among sensors over daylight hours to create a daytime average. We then estimate hourly APAR by multiplying hourly incoming PAR (measured and integrated from 400-700 nm) at the top of canopy (PAR) by the daytime average of fAPAR. Fig S2 shows the mean diurnal cycle for July-August 2017 for each sensor, and the across-sensor average, with APAR data collection beginning on July 13, 2017. We note that APAR measurements are only as representative as the distribution of PAR sensors beneath the canopy; while they are placed within the footprint of SIF (Sec 2.2.3) and fetch of eddy covariance (Sec 2.2.4) measurements, they cannot be a perfect representation of canopy APAR for each eddy covariance and SIF measurement.

2.2.2 Fluorescence parameters

We define and clarify three important quantities that define the relationship between absorbed light and emitted SIF at leaf and canopy scales. ϕ_F is the quantum yield of fluorescence, representing the probability an absorbed photon will be fluoresced. This quantity can be observed at leaf level using PAM fluorimetry or calculated by models as a function of rate coefficients for energy transfer (Sec 2.3.3). SIF_{yield} is the canopy emitted SIF per photon absorbed. The quantity is estimated from models and observations as the ratio of absolute canopy SIF and APAR ($SIF_{canopy}/APAR$). SIF_{yield} is our best attempt to account for the effects of (a) canopy absorbed light and (b) SIF re-absorption within the canopy on the canopy integrated emission of SIF.

238 However, factors such as observation angle, fraction of sunlit/shaded canopy components, and
239 difference in footprint from APAR, necessitates an additional diagnostic variable defined as
240 relative SIF (SIF_{rel}). SIF_{rel} is emitted SIF per reflected radiance in the far red spectrum where SIF
241 retrievals occur (SIF/Ref_{fr}). This is useful because it normalizes for the exact amount of
242 'illuminated' canopy components within the sensor field of view, whereas APAR measurements
243 are integrated for the entire canopy.

244 These quantities represent different but equally important versions of reality. It is difficult for
245 models to exactly reproduce the distribution and timing of sunlight in the canopy as observed by
246 PhotoSpec. While SIF_{rel} removes model-observation differences in illumination, it confounds our
247 interpretation of the relationship with GPP_{yield} , which is derived from APAR. As such, we provide
248 both results to be comprehensive, but note the temporal stability associated with SIF_{rel} as the
249 more physical interpretation of canopy yield for this short period of study.

250 2.2.3 Tower Based Measurements of Solar Induced Chlorophyll Fluorescence (SIF)

251 SIF data has been collected from a scanning spectrometer (PhotoSpec) installed at the AmeriFlux
252 US-NR1 tall tower since June 17, 2017. PhotoSpec sits atop the tower at 26 m above the ground
253 and roughly 15 m above the forest canopy top, transferring reflected sunlight and SIF data
254 collected from the needleleaf canopy through a tri-furcated optical cable to three spectrometers
255 in a shed at the base of the tower. These spectrometers measure far-red fluorescence in the 745-
256 758 nm retrieval window at high spectral resolution ($FWHM = 0.3$ nm) and with a 0.7 deg field of
257 view (FOV), resulting in a 20 cm diameter footprint at nadir on top of the canopy. The far-red SIF
258 data are then scaled to 740 nm for model intercomparison using the first principal component of
259 the spectral shape in Magney et al., 2019a. Photospec scans from nadir to the horizon in 0.7
260 degrees steps at two azimuth directions, with a time resolution of ~20 s per measurement and
261 complete scan time of 20 minutes. For this study, we aggregate scans across all azimuth and
262 elevation angles into hourly, canopy level averages to benchmark model estimates of top of
263 canopy (TOC) or canopy averaged SIF (BETHY only, see Sec 2.3.4.1) at diurnal and synoptic time
264 scales. We refer the reader to Grossman et al. (2018) and Magney et al (2019b) for further details
265 regarding PhotoSpec, implementation at US-NR1, and data filtering, and to Magney et al (2019c)

266 for data access. We focus our model-data analysis on the 2017 growing season (July-August,
267 2017) to maximize overlap between observations of SIF, GPP, and APAR.

268 Diurnal composites of PhotoSpec SIF in 2017 show a late morning peak and afternoon dip (Fig
269 S3A). The afternoon dip is consistent with decreased incoming shortwave, PAR and APAR (Figs S1
270 and S2, respectively). However, we note the retrieved signal from PhotoSpec is also affected by
271 (1) viewing geometry, (2) fraction of sunlit vs shaded leaves (sun/shade fraction, i.e. the quantity
272 of needles illuminated by incident sunlight) due to self-shading within the canopy, and (3)
273 direct/diffuse fraction due to cloud cover. Structural and bidirectional effects lead to different
274 SIF emission patterns depending on view angle and scanning patterns (Yang and van der Tol,
275 2018). The viewing geometry of PhotoSpec (as implemented at NR1 in 2017) causes a higher
276 fraction of illuminated vegetation in the morning, which leads to a 2 to 3 hour offset in the timing
277 of peak SIF (Fig S3A) and incoming far-red reflected radiance within the retrieval window (Fig
278 S3B), from the peak zenith angle of the sun at noon (coinciding with the expected peak in PAR)
279 to late morning. Normalizing SIF by far-red reflected radiance as relative SIF (SIF_{rel} , Fig S3C) and
280 rescaling to SIF (Fig S3D) shifts the peak back to noon and preserved the afternoon dip (albeit
281 with reduced magnitude). SIF_{rel} helps to account for factors 1-3 listed above because it accounts
282 for the amount of reflected radiation in the field of view of PhotoSpec, which is impacted by
283 canopy structure, sun angle, and direct/diffuse light. As discussed above, SIF_{rel} is likely a better
284 approximation of SIF_{yield} because it normalizes for the exact amount of 'illuminated' canopy
285 components in each retrieval, whereas APAR integrates the entire canopy. As such, we expect
286 SIF_{rel} to have a strong seasonal change associated with downregulation of photosynthesis, and a
287 more subtle diurnal change, as during mid-summer the SIF signal is primarily driven by light
288 intensity.

289 It is important to note that the PhotoSpec system is highly sensitive to sun/shade fraction in the
290 canopy (factor 2) due to the narrow FOV of the PhotoSpec telescoping lens. Increased afternoon
291 cloud cover during summer causes diurnal asymmetry in incident PAR (Fig S1A). We examine this
292 effect in more detail (Section 3) by analyzing SIF and GPP under clear and diffuse sky conditions
293 using a threshold (0.5, top-of-canopy/top-of-atmosphere incoming shortwave radiation) similar
294 to that used in Yang et al. (2017) and Yang et al. (2018).

295 2.2.4 CO₂ Flux and GPP Partitioning

296 NEE measurements are screened using u_{star} filtering, and partitioned into gross primary
297 production (GPP) and terrestrial ecosystem respiration components using the so-called nighttime
298 method which is based on the relationship between NEE during the nighttime ($PAR < 50 \mu mol m^{-2} s^{-1}$) and air temperature (Reichstein et al., 2005). Diurnal averages of GPP based on nighttime
299 partitioning show similar diurnal structure to PAR and SIF including the afternoon dip and
300 reduced overall magnitude compared to the 2015-2018 mean (Fig S4). Similar results are found
301 using daytime light partitioning of NEE (Lasslop et al., 2010; Fig S4) and thus only nighttime
302 partitioned GPP data are reported for the remainder of this study. All GPP estimates are
303 processed as half hourly means, then gap filled and averaged hourly. We note the tower location
304 near the Continental Divide in the Rocky Mountains of Colorado presents slope flow challenges
305 for eddy covariance during nighttime, but the relatively flat area of the tower reduces impact on
306 daytime flux measurements (Burns et al., 2018). Details on the flux measurements, data
307 processing and quality control are provided in Burns et al. (2015).

309 2.3 Modeling Approach

310 2.3.1 TBM-SIF Overview

311 The parent TBMs are designed to simulate the exchanges of carbon, water, and energy between
312 biosphere and atmosphere, from global to local scales depending on inputs from meteorological
313 forcing, soil texture, and plant functional type. The addition of a fluorescence model that
314 simulates SIF enables a direct comparison to remotely sensed observations for benchmarking,
315 process diagnostics, and parameter/state optimization (data fusion) for improved GPP
316 estimation. The TBM-SIF models analyzed here differ in ways too numerous to discuss. We refer
317 the reader to the appropriate references in Section 2.3.4 for more detailed model descriptions.
318 Instead, we focus on key differences affecting joint simulation of GPP and leaf/canopy level SIF
319 at diurnal and synoptic scale, during the peak of summer. These differences, which are
320 summarized in Table 1, include the representation of stomatal-conductance (all use Ball-Berry
321 except CLM5.0, BEPS, and ORCHIDEE), canopy absorption of incoming radiation (all account for
322 sunlit/shaded radiation except ORCHIDEE, SiB3, and SiB4), limiting factors for photosynthesis

(V_{cmax} , LAI, radiation, stress) and SIF (k_N , fluorescence photon re-absorption), scaling and radiative transfer methods for transferring leaf-level SIF simulations to top of canopy, and parameter optimization. Further details on (a) photosynthetic structural formulation and parameter choice, (b) representation of leaf level processes important to SIF (k_N and ϕ_P), and (c) leaf-to-canopy scaling approach (SIF_{canopy}) are provided in Sections 2.3.2 and 2.3.3.

2.3.2 Photosynthesis Models

All TBM-SIF models in this manuscript used enzyme-kinetic models to simulate leaf assimilation rate (gross photosynthesis) as limited by the efficiency of photosynthetic enzyme system, the amount of PAR captured by leaf chlorophyll, and the capacity of leaves to utilize end products of photosynthesis (Farquhar et al., 1980; Collatz et al., 1991, 1992; Sellers et al., 1996). However, there are important differences in the representation of (a) stomatal conductance that couples carbon/water cycles, and (b) limiting factors on carbon assimilation due to leaf physiology (maximum carboxylation capacity, V_{cmax}), radiation (APAR or fAPAR), canopy structure (LAI, leaf angle distribution), and stress (water supply and demand, temperature), that affect plant physiological processes and canopy radiative transfer. The underlying stomatal conductance models in the TBMs analyzed here are represented by the Ball-Berry family of empirical models rooted in the leaf gas exchange equation but with different representations of atmospheric demand (relative humidity or vapor pressure deficit), including the Ball-Berry-Woodrow model (Ball et al., 1987), the Leuning model (Leuning, 1995), the Yin-Stuik model (Yin and Struik, 2009), and the Medlyn model (Medlyn et al., 2011). These structural and parametric differences also influence calculated values such as the degree of light saturation (Section 2.3.3), which influence both the fluorescence and quantum yield as used by the fluorescence models. Differences in stomatal conductance, canopy type / radiation scheme, stress, V_{cmax} , and LAI are summarized in Table 1.

2.3.3 Fluorescence Modeling Approach

Following the general approach described in Lee et al. (2015) and van der Tol et al. (2014), the flux of total leaf-level emitted fluorescence, SIF_{leaf} , can be diagnosed using a light use efficiency framework analogous to the expression for photosynthesis (Monteith et al., 1972),

$$\begin{aligned}
SIF_{leaf} &= fAPAR * PAR * \phi_F \\
&= APAR * \phi_F
\end{aligned}
\tag{Equation 1}$$

where PAR and $fAPAR$ are defined in Section 2.2.1 but measured at leaf level, and ϕ_F is the quantum yield of fluorescence, representing the number of photons emitted by fluorescence per absorbed photon. We note that photosystems I and II (PSI and PSII, respectively) contribute to leaf level fluorescence but only PSII is considered in models analyzed here (with the exception of ORCHIDEE and BETHY, Section 2.3.4.2). ϕ_F is estimated as follows:

$$\phi_F = \frac{k_F}{k_F + k_D + k_N} (1 - \phi_P)
\tag{Equation 2}$$

where k represents the rate coefficients for the different pathways for the transfer of energy from excited chlorophyll (k_F = fluorescence, k_D = heat dissipation, and k_N = non-photochemical quenching, or NPQ), and ϕ_P is the quantum yield of electron transport (see Section 2.3.2). k_F is typically set to a constant value (0.05) in models following van der Tol et al (2014). k_D is also typically set to a constant value of 0.95, or temperature corrected in some cases (e.g., ORCHIDEE, CLM4.5, CLM5.0, BETHY). k_N has a substantial and variable impact on energy partitioning at diurnal and seasonal scales which varies as a function of light saturation (e.g., Raczka et al., 2019; Porcar-Castell et al., 2011). Once leaf level emissions are known, an approach is needed estimate the total TOC fluorescence flux (SIF_{canopy}) for comparison to Photospec data. Leaf and canopy level fluorescence modeling is described in more detail in Section 2.3.3.1 and 2.3.3.2 below.

2.3.3.1 Leaf level SIF emission

The ‘quantum yield’ approach has been used in SIF models to characterize the fraction of photons that are used for PQ, NPQ, or re-emitted as fluorescence (van der Tol 2014). It is important to note, that this does not translate into the actual amount of SIF emission leaving the leaf, but is used as an approximation. TBM-SIF models typically represent ϕ_P using lake model formalism, which assumes large connectivity between photosynthetic units (Genty et al., 1989; van der Tol et al., 2014). ϕ_P is expressed in terms of the degree of light saturation (x), derived from the native photosynthesis module of the parent TBM and represents the balance between actual and potential electron transport rates, and the maximum photochemical yield under dark-acclimated

conditions (ϕ_{pmax}), which is derived from the fluorescence model and defined in terms of rate coefficients in Eq 2.

ϕ_N accounts for the ability of plants to dissipate excess energy as heat via NPQ through the regulation of xanthophyll cycle pigments (Demmig-Adams and Adams, 2006). NPQ can be represented as a sum of reversible (k_R) and sustain (k_S) components ($k_N = k_R + k_S$). k_R accounts for the relatively fast (diurnal), reversible NPQ response to light. k_S accounts for the relatively slow (seasonal), sustained NPQ response to light and other environmental factors. With the exception of CLM4.5, models do not typically account for k_S .

A significant challenge in fluorescence models is to find an appropriate relationship between k_N and the degree of light saturation (x). The TBM-SIF models represent k_N through an approach similar to the one used in SCOPE, which uses a parametric model of k_N derived from PAM fluorometry measurements (van der Tol et al., 2014).

NPQ models can be classified as stressed (drought) and unstressed relative to water availability depending on the dataset from which empirical fits are derived. The unstressed model is ideal for irrigated systems such as crops, and the stressed model is more appropriate for water limited ecosystems such as Niwot Ridge. We examine each of these models using drought and unstressed models from van der Tol (2014), and a drought-based model from Flexas et al. (2002). These models use different empirical fits but are otherwise identical. In general, k_N increases more rapidly with APAR (light saturation), and ramps up to a higher level, in the drought-based model compared to the unstressed model. Additionally, some models provide unique improvements such as dependence on environmental conditions (e.g., water stress vs no water stress in ORCHIDEE), and equations for reversible and sustained NPQ to represent the different time scales (minutes to seasonal) at which NPQ regulation occurs (e.g., CLM4.5) influenced by pigmentation changes in the leaf.

2.3.3.2 Leaf-to-Canopy scaling

The TBM-SIFs produce leaf-level fluorescence which needs to be converted to canopy-level fluorescence (SIF_{canopy}) to be directly compared to PhotoSpec and satellite observations. Leaf- to canopy- level conversion of SIF requires a representation of canopy radiative transfer, which in

406 general is too computationally expensive to include within the TBMs in this study, that are
407 designed for global scale application. Therefore, most TBMs analyzed here account for canopy
408 radiative transfer of SIF using some representation of SCOPE (van der tol 2009a,b). The most
409 commonly used approach is to run independent simulations of SIF from SCOPE to create an
410 empirical conversion factor (κ_{740}) between leaf and canopy level SIF that is a function of V_{cmax}
411 (Lee et al., 2015). This conversion factor accounts for integration over the fluorescence emission
412 spectrum, observation angle, and unit conversion. Model variations of this empirical approach,
413 as well additional approaches utilizing the full SCOPE model and a SCOPE emulator, are
414 summarized below and in Table 1.

415 2.3.4 TBM-SIF Models

416 Here we provide a brief description of individual TBM-SIF models and within model experiments.
417 We point out key differences in modeling of photosynthesis, fluorescence, and leaf-to-canopy
418 scaling. We note that within model experiments, labeled as Experiment 1 (exp1), Experiment 2
419 (exp2), etc, represent increasing order of realism, rather than a specific set of conditions common
420 across models. As such, Experiment 1 in BETHY (*BETHY-exp1*) is not equivalent to Experiment 1
421 in CLM4.5 (*CLM4.5-exp1*).

422 2.3.4.1 BETHY

423 The Biosphere Energy Transfer Hydrology (BETHY) model is the land surface component of the
424 Carbon Cycle Data Assimilation System (CCDAS) developed to ingest a range of observational data
425 for estimating terrestrial carbon fluxes at global scale (Rayner et al., 2005; Kaminski et al., 2013;
426 Koffi et al., 2012; Anav et al., 2015). Koffi et al. (2015) was the first to combine a process-based
427 model of SIF with a global TBM. The native canopy radiative transfer and photosynthesis schemes
428 of BETHY were effectively replaced with corresponding schemes and fluorescence model from
429 SCOPE (Koffi et al., 2015), thus enabling spatially explicit simulation of GPP and SIF as a function
430 of plant function type. This model was extended to include a module for prognostic leaf growth
431 (Norton et al., 2018) and more recently adapted with a formal optimization algorithm for
432 assimilating spaceborne SIF data (Norton et al., 2019). It has been updated for this study to accept
433 hourly meteorological forcing. BETHY-SCOPE, denoted here as BETHY, remains the first and only

global TBM-SIF model to simulate vertically integrated (1-D) fluorescence radiative transfer and energy balance.

We include three experiments to examine the impact of calibrating the k_N model against PAM fluorometry data to different species: (1) *BETHY-exp1* is adapted to unstressed cotton species (van der Tol et al., 2014), (2) *BETHY-exp2* is adapted to drought stressed Mediterranean species (i.e., vineyard in controlled environment subjected to drought) including higher temperature correction (Flexas et al., 2002; van der Tol et al., 2014), (3) *BETHY-exp3* is adapted to drought stressed Mediterranean species (Flexas et al., 2002).

We further leverage SCOPE enabled SIF modeling in BETHY (*BETHY-exp3* specifically) to examine (a) leaf and canopy level SIF and quenching under sunlit and shaded leaves, and (b) SIF emissions at the top of canopy (SIF_{canopy}) versus the average emission within the canopy (SIF_{ave}), which accounts for the average emission from sunlit and shaded leaves. The latter analysis facilitates comparison to PhotoSpec, which observes the entire canopy.

An important caveat in the analysis of BETHY simulations is that, at the time of this writing, the prescribed meteorological forcing at NR1 is only available for 2015. While this degrades comparison to diurnal and synoptic variation observed by PhotoSpec in 2017, we find that analysis of magnitude, light sensitivities, and within model experiments still provides useful insight for interpretation of other TBM-SIFs, and future modeling requirements in general.

2.3.4.2 ORCHIDEE

The Organizing Carbon and Hydrology In Dynamic Ecosystems (ORCHIDEE) model (Krinner et al., 2005) is the land surface component of the Earth System Model of Institut Pierre-Simon Laplace IPSL-CM, (Dufresne et al., 2013) involved in recent exercises of the Coupled Model Intercomparison Project (CMIP) established by the World Climate Research Programme (<https://www.wcrp-climate.org/wgcm-cmip>). Recently a mechanistic SIF observation operator was developed for ORCHIDEE to simulate the regulation of photosystem II ϕ_F at the leaf level using a novel parameterization of NPQ as a function of temperature, PAR, and normalized ϕ_P . It emulates the radiative transfer of SIF to the top of the canopy using a parametric simplification of SCOPE. The details of the SIF modelling approach are provided in Bacour et al. (2019).

We include three experiments to examine the impact of water stress and parameter optimization (using OCO-2 SIF, see Section 2.4): (1) *ORCHIDEE-exp1* is the standard configuration with default parameters, (2) *ORCHIDEE-exp2* is the same as *ORCHIDEE-exp1* with two key differences (a) water stress is applied to stomatal conductance, mesophyll conductance and to the photosynthetic capacity, and (b) the tree height (12 m instead of 15 m) was set specifically for the NR1 site, (3) *ORCHIDEE-exp3* is the same as *ORCHIDEE-exp1* but includes OCO-2 optimized parameters.

2.3.4.3 BEPS

The Boreal Ecosystem Product Simulator (BEPS) is an enzyme kinetic two-leaf model for simulating carbon and water cycles for different plant functional types (Chen et al., 1999; Liu et al., 2003). BEPS uses a modified Ball-Berry stomatal conductance model (Leuning et al., 1995) and semi-analytical canopy radiative transfer. The canopy architecture is well considered in BEPS model, which has not only remote-sensed LAI but also the global map of the foliage clumping index. The fluorescence emission at the leaf level follows the approach of Lee et al (2015). SIF emission for sunlit and shaded leaves are separately simulated based on illumination and canopy geometry in BEPS. In addition, multiple scattering SIF is also simulated to account for the scattering process within the canopy. The scaling of leaf-level fluorescence emission to the canopy is based on a novel scheme for single-layer models which accounts for canopy scattering and extinction from sunlit and shaded leaves (Qiu et al., 2019). This scaling scheme is an effective approach to simulate the radiative transfer of SIF for a given canopy structure. We include two experiments similar to *BETHY-exp1/2* in the calibration of the k_N model against unstressed vs stressed species (*BEPS-exp1* and *BEPS-exp2*, respectively).

2.3.4.4 CLM4.5

The Community Land Model version 4.5 (CLM4.5) provides a description of the biogeochemical profile spanning from the sub-surface bedrock to the top of the vegetation canopy. The fluorescence sub-model follows Raczka et al. (2019), in which the degree of light saturation is calculated from the potential and actual electron transport rate as determined from the photosynthesis model described above. ϕ_f is formulated as described in Equation 2 and ϕ_p is formulated as a function of the maximum ϕ_p under dark acclimated conditions and the degree

of light saturation. CLM4.5 uses independent site-level SCOPE simulations that match the observed canopy characteristics and observed GPP at Niwot Ridge to calculate a leaf to canopy level conversion factor (κ_{740}) for estimating SIF_{canopy} . In CLM4.5, κ_{740} is fitted to the modeled SCOPE data as a function of solar zenith angle (and implicitly V_{cmax}).

Similar to Raczka et al. (2019), here we examine three separate approaches to parameterize k_N . *CLM4.5-exp1* only considers reversible NPQ (k_R), such that, $k_N = k_R$, and the relationship between k_R and the degree of light saturation is fitted to PAM fluorometry data based on Mediterranean shrubs (Flexas et al., 2002; Galmes et al., 2007). *CLM4.5-exp2* parameterizes k_R with PAM fluorometry from a Scots Pine forest (Porcar-Castell et al., 2011), and defines the rate coefficient in terms of both a reversible and sustained component ($k_N = k_R + k_S$). It has been found that sustained NPQ is important for cold climate evergreen conifer forests such as Niwot Ridge (Miguez et al., 2015; Magney et al., 2019b), and Raczka et al. (2019) found that representing both components provided improved simulations of seasonal SIF. *CLM4.5-exp3* is similar to *CLM4.5-exp2* but includes a seasonally varying representation of k_R . All model experiments use hand-tuned parameters specific to US-NR1 (Raczka et al., 2016).

2.3.4.5 CLM5.0

CLM version 5.0 (CLM5.0) is similar to CLM4.5 with respect to the implementation of the fluorescence sub-model, yet includes several important updates to the representation of photosynthesis from CLM4.5, including a prognostic calculation of V_{cmax} based upon leaf nitrogen and environmental conditions, revised nitrogen limitation scheme, Medlyn stomatal conductance model, and plant hydraulic water stress (Kennedy et al., 2019). To represent NPQ we use a single approach for k_N (see *CLM4.5-exp1*), but examine three approaches for estimating κ_{740} : (1) *CLM5.0-exp1* uses κ_{740} as function of V_{cmax} following Lee et al (2015), (2) *CLM5.0-exp2* follows the approach of *CLM4.5*, and (3) *CLM5.0-exp3* adapts the approach proposed by Zeng et al. (2019) that estimates the fraction of total emitted SIF escaping the canopy by combining near-infrared reflectance of vegetation (NIR_v) and fPAR.

2.3.4.6 SIB3

517 The Simple Biosphere Model version 3 (SIB3) involves the use of explicit biophysical mechanisms
518 to directly calculate carbon assimilation by photosynthesis (Baker et al., 2003; 2008). SiB3
519 includes prognostic calculation of temperature, moisture, and trace gases in the canopy air space,
520 but requires prescription of most structural properties including LAI. We examine two
521 approaches for prescribing LAI: (1) *SIB3-exp1* using values prescribed from MODIS, and (2) *SIB3-*
522 *exp2* uses values observed at the study site ($4.0 \text{ m}^2 \text{ m}^{-2}$). In general, the fluorescence sub-model
523 follows the approach of Lee et al. (2015) except that k_N is adapted to drought stressed species
524 following van der Tol et al (2014).

525 2.3.4.7 SIB4

526 SIB4 (Haynes et al., 2019a,b) shares many similarities to SIB3 with respect to functional aspects
527 of photosynthesis and fluorescence, however, SIB4 uses prognostic rather than prescribed
528 phenology and LAI.

529 2.3.5 SCOPE

530 SCOPE is a multi-layer canopy model which explicitly represents the within canopy radiative
531 transfer of fluorescence, whereas TBM-SIFs analyzed here (with the exception of BETHY) only
532 provide an empirical representation. We provide results from a stand-alone version of SCOPE
533 v1.73 (van der Tol et al., 2014) as an additional benchmark for TBM-SIF simulations of APAR, GPP,
534 SIF, and quantum yields. There are three important reasons for this: (1) It is inherently difficult
535 to provide representative and accurate *in situ* measurements of APAR, SIF, and GPP for
536 comparison to models; (2) SCOPE provides estimates of quantum yields for fluorescence,
537 photochemistry, and non-photochemical quenching, which are not measured continuously in the
538 canopy at NR1; and (3) SCOPE offers a more direct benchmark for evaluating more simplified
539 representations of canopy radiative transfer in TBM-SIFs. Unlike the TBM-SIFs, SCOPE does not
540 include a representation of biogeochemical cycling or carbon pools, and thus no spin up is
541 required. As such, we prescribe LAI ($4 \text{ m}^2 \text{ m}^{-2}$), canopy height (13 m), and leaf chlorophyll content
542 (25 ug cm^{-2}) following Raczka et al. (2019). We also examine two approaches for prescribing V_{cmax} :
543 (1) *SCOPE-exp1* uses the default constant value of 30, similar to *BETHY*, and (2) *SCOPE-exp2* uses
544 a seasonal varying value calibrated to NR1, following Raczka et al. (2016, 2019), which follows a

545 bimodal distribution peaking near 45 in early summer (DOY = 150) and 40 in late summer (DOY =
546 250)

547 2.4 Data Assimilation

548 Details of the data assimilation protocols for ORCHIDEE is provided in Bacour et al. (2019). An
549 ensemble of parameters related to photosynthesis (including optimal V_{cmax}) and phenology were
550 optimized for several plant functional types. Note that none of the assimilated pixels encompass
551 the location of the US-NR1 tower. In ORCHIDEE, the study site is treated as boreal needleleaf
552 evergreen (ENF); as such, the *ORCHIDEE-exp3* simulations in this study are based on parameters
553 optimized against OCO-2 SIF data using an ensemble of worldwide ENF pixels. Note that for
554 BETHY, each experiment uses the same set of optimized parameters whereas in ORCHIDEE the
555 SIF simulations are performed separately for the standard parameters (*ORCHIDEE-exp1/exp2*)
556 and optimized parameters (*ORCHIDEE-exp3*), thus providing a test of sensitivity to parameter
557 optimization as discussed below.

558 2.5 Illumination Conditions

559 In order to gain insight into how SIF emissions and quantum yields vary with illumination, we
560 further analyze Photospec and a subset of models with respect to (a) changes in incoming light
561 and (b) self-shading within the canopy, respectively. For PhotoSpec, we analyze changes in
562 canopy average SIF and SIF_{rel} under conditions of predominantly direct versus diffuse PAR, using
563 a 0.5 threshold to distinguish between the two conditions (Section 2.2.3). For models we focus
564 on emissions from sunlit vs shaded leaves. We analyze leaf- versus canopy-level SIF emissions
565 (SIF_{leaf} and $\text{SIF}_{\text{canopy}}$) in *CLM4.5-exp3*, and leaf-level quantum yields (ϕ_f , ϕ_p , ϕ_N) in *SCOPE-exp2*.
566 We further compare predictions of quantum yield at the top-of-canopy to canopy averages in
567 *SCOPE-exp2*. The motivation here is that top-of-canopy leaves see most of the sunlight, and thus
568 should have different yields compared to shade adapted leaves lower in the canopy. This also
569 provides a more direct comparison for PhotoSpec.

570 2.6 Modeling Protocol

571 Models are run for the period 2000-2018 (except BETHY (2015 only) and SCOPE (2017 only)) using
572 identical, hourly, gap-filled meteorological observations. The primary hourly output fields

analyzed are the top-of-canopy SIF ($\text{SIF}_{\text{canopy}}$ @ 740 nm), GPP, ϕ_f , ϕ_p , and APAR. Model-observation comparisons are made for absolute and relative SIF, GPP, $\text{SIF}_{\text{yield}}$ ($\text{SIF}_{\text{canopy}}/\text{APAR}$) and $\text{GPP}_{\text{yield}}$ (GPP/APAR), sunlit versus shaded canopies (*CLM4.5-exp3* and *SCOPE-exp2*), and TOC versus canopy average SIF ($\text{SIF}_{\text{canopy}}$ versus SIF_{ave} , respectively, from *SCOPE-exp2*). Quantum yields and within model experiments provide context to understand canopy integrated results. We focus our analysis on 8 am – 4 pm local time from July-August 2017 for comparison to available PhotoSpec and APAR data.

Models are controlled for meteorological forcing (meteorological data described in Burns et al., 2015) but other factors such as spin-up, land surface characteristics, parameter tuning, and model state, are not controlled for and are treated separately according to each model's protocol. For example, CLM4.5 is better suited than others in prescribing observed vegetation characteristics at the study site. One ORCHIDEE experiment (*ORCHIDEE-exp3*) is preliminary optimized by assimilating independent Orbiting Carbon Observatory 2 (OCO-2) SIF data at the global scale (Section 2.4). We emphasize that our point here is not to identify the best model but to identify common patterns in model behavior through normalized SIF and deviation from observed behavior to identify areas requiring the most attention.

The results are organized around two parallel themes. The first theme addresses four key processes driving canopy-level fluorescence: (1) incoming illumination, (2) energy partitioning on incoming light between photochemistry, fluorescence, and NPQ, and (3) leaf-to-canopy emitted SIF, including linearity of yields at leaf and canopy scale. The second theme addresses sensitivity of these processes to environmental conditions at diurnal and synoptic scales. Here, synoptic scale refers to the impact of day-to-day changes in weather, including two storm events which brought sustained cool, wet, and cloudy conditions from July 22-31 and then from August 6-10.

Section 3: Results

Incoming Illumination

Two key features dominate observed APAR variability: afternoon depression (Fig 2A) and reduction during two summer storms (Fig 2D). Both features are captured by models. More generally, models capture synoptic variability with high correlation ($r > 0.8$) and low across model

601 spread ($\sigma = 10\%$). The exception is BETHY, which is simulated outside our observation year (2015).
 602 High model fidelity is expected given that observed PAR is prescribed, and it is promising that
 603 models show a consistent response to changes in illumination. The primary shortcoming across
 604 TBM-SIFs and SCOPE is a systematic high bias in APAR magnitude (129%), with most models
 605 exceeding the upper range of observed APAR (as determined from the six within canopy PAR
 606 sensors, Fig S2), and high model spread. These errors are likely related to differences in predicted
 607 fAPAR. In the case of ORCHIDEE, high APAR is expected due to the big leaf assumption where all
 608 leaves are considered as opaque and fully absorbing.

609 *Canopy Photosynthesis*

610 Observed GPP shows a broad peak from mid-morning to early afternoon (~9 am – 1 pm local),
 611 followed by slight decrease until 4 pm (Fig 2B), consistent with afternoon cooling and reduced
 612 light availability (Fig 1B-D). The two month period under investigation is relatively flat with
 613 generally weak day-to-day variability ($\sigma = 17\%$), but modest correlation with APAR ($r = 0.61$, Fig
 614 2E). Some models capture the afternoon GPP depression, but all models strongly underestimate
 615 its magnitude, apparently independent of stomatal conductance formulation or more explicit
 616 accounting for plant hydraulic water stress such as in CLM5.0. *SCOPE* and *BETHY*, which don't
 617 account for water stress, show no afternoon depression. Models are mostly uncorrelated with
 618 observed GPP at synoptic scale (r ranges from -0.2 to 0.36, highest value in SiB4), high biased,
 619 and show increased spread (in predicted magnitude) relative to APAR (143% +/- 23%). *SCOPE-*
 620 *exp2* shows slight improvement in GPP magnitude with the larger V_{cmax} value in late summer.

621 While observed GPP_{yield} is mostly stable over the diurnal cycle, most models (except BEPS) show
 622 a distinct midday minimum (Fig 3A). Half of the models show a similar midday minimum in
 623 photochemical quantum yield (ϕ_P , Fig 4A), with the other half either increasing or decreasing in
 624 the afternoon (CLM5.0 and SiB3/SiB4, respectively). The midday dip in yield is likely associated
 625 with reduced photosynthetic efficiency at high light levels, as demonstrated by reductions in GPP,
 626 GPP_{yield} , ϕ_P with APAR (Fig 5A, C, E).

627 Observed GPP_{yield} shows significant structure at synoptic temporal scale (Fig 3C), most notably
 628 increased yield during the cool/rainy period (reduced heat and water stress), and decreased yield

in mid- to late- August (increased heat and water stress following the cooling pattern). In contrast to predicted GPP, models show high fidelity in capturing the magnitude and variability of GPP_{yield} at synoptic scale (r ranges from 0.35 – 0.76, highest values in *SCOPE* and *CLM4.5/5.0*). Individual models are self-consistent in their predictions of GPP_{yield} and ϕ_P at synoptic scale ($r = 0.592 - 0.935$) except for SiB3/SiB4 ($r < 0.1$, Fig 4B).

Canopy Fluorescence

Observed SIF_{canopy} is strongly correlated with observed APAR at diurnal and synoptic scale ($r = 0.77$), with common features including afternoon depression and reduction during rainy periods (Fig 2C & 2F). Observed PAR also feeds into the fluorescence sub-model and, unlike GPP, strongly correlates with SIF_{canopy} at synoptic scale (r ranges from 0.58 to 0.92, highest values in *SCOPE* and *ORCHIDEE*). However, we find a persistent positive model bias in SIF_{canopy} (170% +/- 45%) consistent with, but not proportional in magnitude to, the APAR bias. We note that models are especially oversensitive to APAR at high light levels (Fig 5D).

We investigate the high bias in SIF_{canopy} in more detail using *SCOPE-exp2* and *CLM4.5-exp3*. Specifically, we examine leaf and canopy level SIF and quenching under sunlit and shaded leaves. Analysis of quantum yields in *SCOPE-exp2* (Fig S5) shows a reversal in the fractional amounts of absorbed energy going to SIF and PQ vs NPQ in low- vs high-light conditions that is consistent with leaf level data and theory (Porcar-Castell et al., 2014). More specifically, *SCOPE-exp2* predicts low ϕ_F and ϕ_P and high ϕ_N in sunlit leaves relative to shaded leaves, with more energy going to fluorescence and photochemistry than to NPQ in shaded leaves, and more energy going to (shed off by) NPQ in sunlit leaves (Fig S5). Likewise, total ϕ_F shows decreasing values with increasing APAR in *SCOPE* and *BETHY-exp2/3* compared to *BETHY-exp1*, consistent with observed SIF_{yield} (Fig 5E-F), as ϕ_N ramps up to higher levels in the drought parameterized Kn model. Moreover, in stark contrast to SIF_{yield} and SIF_{canopy} , ϕ_F does not show high values relative to other models (Fig 4D). These results point to an issue in *SCOPE* and *BETHY* with leaf to canopy scaling in needleleaf forests.

Analysis of *CLM4.5-exp3* suggests several possible reasons for oversensitivity to APAR. First, we focus on emissions from sunlit/shaded portions of the canopy (Fig S6). *CLM4.5-exp3* and

657 PhotoSpec both show higher SIF under “high light” conditions (sunlit leaves and direct radiation,
658 respectively) compared to “low light” conditions (shaded leaves and diffuse radiation,
659 respectively), which is promising (Fig S6 A,D). Comparing the ratio of sunlit to shaded SIF in
660 *CLM4.5-exp3* to the ratio of direct to diffuse SIF in PhotoSpec (Fig S6 B,E) shows higher ratio in
661 *CLM4.5-exp3* on average. The difference peaks in midday, when sunlit leaf area is maximized
662 (self-shading minimized) in CLM4.5 but no major difference in the amount of direct radiation,
663 and decreases with increasing sun angle (morning and afternoon) and with increasing rainfall (in
664 the afternoon on average, and during the rainy period in late July / early August), both of which
665 increase the shaded fraction. As such, accounting for view angle and different illumination
666 metrics for PhotoSpec and CLM4.5 (most comparable in morning, afternoon, and during rainy
667 days) reduces, but does not entirely remove, the positive bias in high light conditions.

668 Second, the degree of light saturation (x) is twice as high in the sunlit canopy in *CLM4.5* (Fig S7),
669 which leads to low fluorescence efficiency in sunlit leaves and high fluorescence efficiency in
670 shaded leaves. While this produces high photochemistry in shaded leaves, it contributes a small
671 fraction of SIF to the total canopy ($\sim 20\%$) despite higher fractions of shaded leaves ($\sim 2/3$ at noon,
672 Fig S6C) and thus sunlit leaves dominate SIF_{yield} and SIF_{canopy} . Therefore, it seems likely that a
673 model’s representation of canopy structure including the partitioning between sunlit/shaded leaf
674 area fractions has an important impact upon canopy SIF. Biases in the sunlit/shaded fraction will
675 likely propagate into the simulated value of canopy SIF. However, it’s important to know that the
676 observed sunlit/shaded fraction from PhotoSpec is estimated as well, since it is currently not
677 possible to determine the precise sun/shade fraction within PhotoSpec FOV.

678 Additionally, all formulations of CLM4.5 (and most models except BETHY and SCOPE) show lack
679 of decline in SIF_{yield} with APAR compared to measurements of absolute SIF (Fig 5E). For CLM4.5,
680 the relationship between SIF_{yield} and APAR depends upon the relationship between degree of
681 light saturation and reversible NPQ (Raczka et al., 2019). This suggests it is important to properly
682 represent the NPQ response to environmental conditions when simulating SIF.

683 While most of the model bias is reduced in SIF_{yield} (126%, mostly attributed to BETHY and SCOPE),
684 the remaining signal, representing the dynamic response to synoptic conditions (e.g., Magney et
685 al., 2019), is poorly represented in models, as demonstrated in a time series of 5-day means (Fig

3D). Most models show zero to strongly negative correlation with observations at synoptic scale and only three models (*SCOPE*, *ORCHIDEE-exp3*, and *BETHY-exp2/3*), produce correlation greater than 0.5. These are the only three models that also capture a negative relationship between SIF_{yield} and APAR (Fig 5E).

In general, predicted SIF_{yield} is stable during our short study period (Fig 3). Half of models show a significant positive correlation with GPP_{yield} ($r > 0.85$) and half show zero or negative correlation (Fig S8). While these findings run counter to observed SIF_{yield} , which shows a clear response during and following the storm event and moderate positive correlation with observed GPP_{yield} ($r = 0.40$), they show some consistency with observed SIF_{rel} (grey line in Fig 3 and Fig S8A) which like many models is stable and uncorrelated with GPP_{yield} . We refer the reader to Section 2.2.2 for clarification of the important difference between SIF_{yield} and SIF_{rel} .

Leaf-to-Canopy Scaling

Several methods have been proposed to transfer predicted leaf-level SIF emissions to the top of canopy. While leaf-to-canopy scaling enables efficient global scale simulation, the diversity of novel methods adds uncertainty to the canopy level estimate of SIF (in addition to aforementioned uncertainties in structure, APAR, photochemistry, fluorescence). These differences are evident in comparison of Figures 3 and 4, in which yields are plotted on a similar scale.

At least at diurnal scale, there is some evidence that leaf and canopy emissions look more similar for models adopting simplified empirical scaling functions (SiB3, SiB4, CLM4.5, CLM5.0, BEPS) than for models that more explicitly account for radiative transfer (*SCOPE*, *BETHY*, *ORCHIDEE*). For the more explicit models, the diurnal cycle of ϕ_f is out of phase with SIF_{yield} , the former of which peaks in the afternoon and the latter of which peaks in the morning. This produces reasonable agreement to PhotoSpec in phase and magnitude between SIF_{yield} and SIF_{rel} for *ORCHIDEE*, but produces divergence in the magnitude of SIF_{canopy} for *ORCHIDEE*.

Model performance in leaf-to-canopy scaling is summarized in Figure S8. The only three models with a positive relationship between yields (Fig S8B) and between quenching terms (Fig S8C) include explicit representation of radiative transfer (i.e., *SCOPE*, *BETHY*, and *ORCHIDEE*). CLM4.5

714 is the only model with a positive relationship between yields, but not between quenching terms.
715 SiB3/SiB4 are the only models with a positive relationship between quenching terms, but not
716 between yields.

717 Finally, we clarify an important difference between observed and predicted estimates of canopy
718 average SIF. PhotoSpec scans direct emissions from sunlit and shaded leaves within the canopy,
719 thus observing the ‘total’ emission from leaves in the instrument FOV. We then average each of
720 these leaf-level scans and report as canopy averages. Model output, in contrast, is reported at
721 the TOC, which represents the ‘net’ emission from leaves after attenuation in the canopy
722 (through canopy radiative transfer, re-absorption of SIF, and shading). Assuming sunlit and
723 shaded leaves within the canopy emit at the same rate as TOC leaves, attenuation will reduce the
724 effective signal from leaf-level emissions within the canopy. As such, the average of leaf level
725 emissions (canopy average) is expected to be lower than the net emission of leaves reaching the
726 top of canopy.

727 This is important because CLM4.5 shows strong attenuation of SIF from leaf-level to TOC,
728 decreasing by a factor of 2-3 at midday (Fig S7). The interpretation here is that the model bias in
729 absolute SIF may actually be higher than reported here; however, we note that more quantitative
730 information on the observed fraction of sunlit vs shaded leaves and comparative top-of-canopy
731 SIF values for the same canopy elements are needed (to account for off-nadir SIF viewing) for
732 more accurate determination of scaling between observed canopy and top-of-canopy SIF.

733 *Within Model Experiments*

734 In most cases, within model experiments produce improvements in some metrics and
735 degradation across others (performance change is quantified by reporting correlation values in
736 brackets). An important and unexpected result of this study is the impact of different levels of
737 tuning to observations on our predictions. While this work represents a snapshot of the state-of-
738 the-art in site-level TBM-SIF modeling, and we have taken great care to control for environmental
739 conditions (most important being illumination), an important overall takeaway is for future
740 model comparisons to make additional efforts to control for initial conditions and vegetation
741 state (i.e. model biophysical parameters).

742 The most basic example is tuning of LAI in SiB3 and V_{cmax} in SCOPE. LAI, as prescribed by MODIS
743 for *SiB3-exp1* (~1.5), is on the low end for a subalpine evergreen forest, and consequently
744 produces negative biases in APAR, GPP, SIF and SIF_{yield} . When prescribed according to tower
745 observations in *SiB3-exp2* (~4.0), the biases become positive (albeit on the lower end of the
746 model ensemble), but produces degraded variation at synoptic scale for GPP (0.39 vs 0.19), SIF
747 (0.87 vs .71) and SIF_{yield} (0.09 vs -0.32). The tuning of V_{cmax} in SCOPE improves the magnitude of
748 GPP, with minimal impact on variability at diurnal- to synoptic- scale.

749 Experiments in CLM4.5 comprise a higher level of hand tuning of vegetation structural and
750 functional characteristics. Parameter tuning was imposed to match vegetation structure with
751 site level measurements and consequently CLM4.5 produces overall low bias in yields. With
752 respect to synoptic variation, NPQ experiments, tuned against the measured air temperature and
753 a representative evergreen forest, produce improvements at synoptic scale for GPP (-0.01 vs
754 0.16), SIF (0.59 vs 0.86), and GPP_{yield} (0.05 vs 0.63), but degradation in SIF_{yield} (0.32 vs -0.25).
755 Likewise, NPQ experiments in BETHY based on species information (calibration of K_N against PAM
756 fluorescence in stressed vs unstressed systems) shows improvement in the SIF_{yield} -APAR
757 relationship for drought stressed models (*BETHY-exp1* vs *BETHY-exp2/3*).

758 Experiments with ORCHIDEE demonstrate that errors in model parameters (such as V_{cmax} , LAI_{max} ,
759 leaf age, or SLA) contribute to SIF and GPP uncertainty but can be alleviated by assimilation of
760 OCO-2 SIF retrievals (*ORCH-exp1/2* vs *ORCH-exp3*). Model optimization of parameters improves
761 the functional link between SIF and GPP, thus reducing biases in APAR, GPP, and SIF_{yield} , and
762 improving synoptic variation in SIF_{yield} (-0.04 vs 0.58).

763 **Section 4. Discussion**

764 This study represents a first attempt to evaluate a controlled ensemble of TBM-SIF models
765 against canopy integrated SIF observations to identify and attribute model-observation
766 mismatches related to errors in canopy absorption of sunlight, photosynthesis, fluorescence, and
767 leaf-to-canopy radiative transfer of fluorescence.

768 Different models match some observed parameters better than others (with respect to APAR and
769 yield), but no model gets both APAR and SIF_{yield} magnitude and/or sensitivities close to the

observations. For example, BEPS closely matches the magnitude of APAR (Fig 2A), and BETHY captures the decline in SIF_{yield} with APAR for NPQ quenching based on stressed species (Fig 5E), but both models overestimate observed yield by a factor of 2, hence SIF is overestimated (Fig 2). CLM4.5 correctly captures the diurnal SIF_{yield} change, but overestimate APAR; in this case, SIF and SIF_{yield} are overestimated. Importantly, models diverge strongly from each other and from observations in the magnitude of SIF_{yield} and its decline with APAR (Fig 5E), partially reflecting model variability in ϕ_f (Fig 5F), but in general show a characteristic pattern of weak SIF_{yield} decline with APAR. GPP_{yield} shows higher agreement between models and with observations (Fig 5B), despite divergent ϕ_p (Fig 5C), which could be indication that the primary uncertainty is due to the representation of fluorescence and not the photosynthesis model.

Consequently, we find a strong linear and positive relationship between observed SIF_{yield} and GPP_{yield} for absolute SIF, which is underestimated on average by models (Fig S8A-B). In contrast, models show quite strong positive relationships between ϕ_f and ϕ_p (Fig S8C). Our study highlights an apparent challenge for models in transferring leaf level processes to canopy scale, and consequently, linking the proper canopy mechanistic SIF-GPP relationship at the leaf level.

The mismatch between multi-model simulations and tower-based observations of SIF and GPP at hourly and daily scales can be summarized as symptoms of five main factors: (1) PhotoSpec scan strategy, (2) radiative transfer of incoming PAR and impact on APAR and sunlit/shaded fraction, (3) representation of photosynthesis and sensitivity to water limitation especially during afternoon conditions, (4) representation of fluorescence and sensitivity to reversible NPQ response at Niwot Ridge, and (5) radiative transfer of fluorescence from leaf to canopy. Several persistent biases falling under these broad categories are discussed below.

Apples to Apples Comparison.

PhotoSpec is unique in its ability to scan entire canopies for signals that are largely hidden from nadir-oriented instruments. However, this creates unique challenges for interpretation of data and comparison to models. For example, the diurnal cycle of observed SIF is highly sensitive to view angle. PhotoSpec was set up in 2017 to scan back-and-forth between northwest and northeast view angles, but the instrument was slightly biased to the northwest, causing a low

798 phase angle in the morning (more aligned with rising sun) and increased phase angle in the
799 afternoon (more opposed to setting sun). As such, PhotoSpec observed predominantly
800 illuminated canopies in the morning and shaded canopies in the afternoon (i.e., more shaded
801 fraction), leading to the late morning peak in reflected radiance (Fig S3).

802 Moreover, Photospec scans specific locations at the top of the canopy from near nadir to view
803 angles closer to the horizon (see Fig. S8 in Magney et al., 2019b), while models are currently
804 configured to simulate top of canopy emission and simulated here as nadir viewing. The question
805 becomes whether to retain nadir only data and sacrifice signal-to-noise, or to average over all
806 elevation angles and risk aliasing view angle effects. This study, partly motivated by high
807 agreement of canopy integrated SIF with spaceborne data from OCO-2 and TROPOMI (Magney
808 et al., 2019b; Parazoo et al., 2019), has chosen the latter approach but with an attempt to
809 minimize scan angle effects in SIF_{rel} . However, it is worth noting that swath sensors such as
810 GOME-2 show high sensitivity to viewing angle especially under increasing illumination angles
811 (Kohler et al., 2018; Joiner et al., in review). View angle effects are likely to be especially acute
812 for PhotoSpec in the morning and afternoon with increasing anisotropy and changes in the
813 illuminated field of view with sun and view angle. Other tower SIF instruments with a wide FOV
814 (i.e. FluoSpec2; Yang et al., 2018) may more appropriately represent the TOC SIF emission, but
815 also have difficulty disentangling the sunlit/shaded canopy components.

816 It is critical that model evaluation relative to measured SIF data and data assimilation studies
817 properly account for the specificities of the instrument (viewing of the instrument, spectral band,
818 time of the overpass for space-borne instruments), the representation of canopy emission, and
819 correct observations for directional variations in SIF relative to observation geometry. Although
820 normalizing SIF by reflected radiance partially alleviates scan angle effects, this highlights the
821 need for models to get canopy structure, radiative transfer, and sunlit/shaded fraction correct,
822 which feed all the way through to SIF and GPP. Further ground-based investigations of SIF
823 anisotropy, sunlit/shade fraction, and vertical distribution (within canopy, canopy integrated,
824 and top of canopy) with PhotoSpec and SCOPE may help to inform models on the physical aspects
825 of the signal. Despite the issues we highlight in comparing observations to models, the potentially

826 more interesting and important story here is with respect to model-model comparisons, which
827 reveals wide divergence in response to light conditions and other factors, as discussed below.

828 **TBM SIF is too sensitive to APAR.**

829 Our results indicate a wide range of SIF responses to APAR: TBM-SIFs and SCOPE are usually far
830 too sensitive to APAR, observations of absolute SIF are less sensitive, and observations of relative
831 SIF (SIF_{rel}) are least sensitive (Fig. 5D). We remind the reader that SIF_{rel} is normalized by the
832 amount of far-red light reflected from leaves in the FOV of PhotoSpec, and thus has reduced
833 sensitivity to absorbed light than absolute SIF. The fact that SIF_{rel} is the least sensitive to APAR
834 means other processes are driving changes in SIF under increased light absorption. In this case,
835 it reveals a strong SIF response to changes in photochemical quenching. SIF models appear
836 especially sensitive to sunlit leaves. In CLM4.5, SIF emissions from the sunlit portion of the canopy
837 are a factor of 5 higher than emissions from shaded leaves, despite twice as fewer leaves in the
838 sunlit canopy (Fig S6C). In CLM4.5, the combination of higher than average ϕ_f (Fig 5F) with higher
839 fluorescence efficiency in the sunlit portion of the canopy, produce an increase in the magnitude
840 and sensitivity to sunlit fraction, thus contributing to the high bias (factor of 3 higher than
841 observed) and strong diurnal cycle (2-fold increase from morning to midday).

842 **Linearity of SIF and GPP yields.**

843 Observations show a positive but not significant linear relationship between SIF_{yield} and GPP_{yield}
844 (Fig 6A, $r = 0.40$) at our study site. This is likely due to the short time period investigated here
845 where there is relatively little change in SIF_{yield} and GPP_{yield} during peak summer. Half of models
846 (4 of 8) show a significant ($r > 0.35$) linear and positive slope ($r > 0.35$; SCOPE, ORCH-exp3,
847 CLM4.5-exp3, and BETHY-exp3) between SIF_{yield} and GPP_{yield} , while 6 models (except CLM5.0)
848 show a significant positive slope between quantum yields (ϕ_f and ϕ_p , Fig S8C). These regression
849 plots of quantum yields, in turn, help explain the observed linearity of SIF_{yield} vs. GPP_{yield} : At least
850 in the case of Niwot Ridge, model (and presumably observed) ϕ_p stays within high light “NPQ-
851 Phase” conditions, and generally doesn’t exceed the range in which decoupling of ϕ_f and ϕ_p (ϕ_p
852 > 0.6) in low light “PQ-Phase” conditions occurs (Porcar-Castell et al., 2014, cf Fig 9). SCOPE and
853 BETHY-exp3, which best capture the observed relationship in the canopy between SIF_{yield} and

Deleted: s

GPP_{yield}, are also the only models that also show a decline in SIF_{yield} with APAR, as discussed below.

These results are likely to change when we expand the study to several years; however, the purpose of this study was to provide an initial investigation into the response of modelled SIF and GPP to light during peak summer.

Insufficient decline in SIF_{yield} with APAR.

In general, models show an insufficient decline in SIF_{yield} with APAR, when compared to observed SIF_{yield} (Fig 5E). All models except SiB3 and SiB4 show some decline, with BETHY showing the best agreement in slope magnitude. SCOPE and BETHY are the only models with full radiative transfer but this does not appear to have a substantial impact on SIF_{yield}, which has a similar (albeit suppressed) decline with APAR as ϕ_f (Fig 5F). Within model experiments show little to no sensitivity of SIF_{yield} or ϕ_f decline with APAR to water stress (e.g., ORCHIDEE) or prescribed LAI (e.g., SiB3), but high sensitivity to the formulation of NPQ with respect to species calibration (e.g., BETHY) and reversibility (e.g., CLM4.5).

Three CLM4.5 experiments demonstrate sensitivity to representation of NPQ variability at diurnal and seasonal scales. The first simulation using the default NPQ parameterization from SCOPE (*CLM4.5-exp1*, based on a 2-parameter fit to drought stressed Mediterranean species (Galmes et al., 2007) produces the strongest decline in SIF_{yield}. The second simulation, which includes a site-specific NPQ formulation that accounts for k_R and k_S (*CLM4.5-exp2*), produces the weakest decline. The third simulation with seasonally varying k_R produces a slightly stronger decline. An important point for this formulation is that k_R is constrained by PAM fluorometry data at Hyytiälä (Scot Pine) and does not account for high light saturation values and summer drought conditions that may be more typical of lower latitude sites such as Niwot Ridge. This could indicate that parameterizing k_R based upon similar PFTs may not be sufficient to properly characterize the NPQ response for lower latitude sites such as Niwot Ridge.

Similar results are found in experiments with BETHY comparing stressed (drought) and unstressed (relative to water availability) NPQ models at NR1 but controlling for k_R (constant in time in both cases, stronger negative SIF_{yield} response to APAR in stressed model). In the unstressed models of CLM4.5 and BETHY, the NPQ response to APAR becomes too low, causing

an oversensitivity of SIF to APAR and thus high SIF bias. The strongly regulated NPQ response of the drought-based model enables more non-photochemical quenching at high light levels in stressed ecosystems compared to typical unstressed plants. While this k_{NPQ} model was developed using drought-stressed plants, similar up-regulation of NPQ is expected to occur under any condition where photosynthesis is limited and available excitation energy is high (e.g. cold temperatures and high light, Sveshnikov et al., 2006). Our results thus emphasize the need for careful implementation of NPQ dynamics for simulating and assimilating SIF in different light and stress environments (Raczka et al., 2019; Norton et al., 2019).

Data assimilation reduces high bias. Assimilation of OCO-2 SIF in ORCHIDEE brings the magnitude of both GPP and SIF in closer agreement with observations. This improvement is driven by decreases in leaf photosynthetic capacity (V_{cmax} , LA_{lmax} , leaf age, SLA, Bacour et al., 2019), which decreases the magnitude (but not shape) of APAR closer to observed values (Fig 2), and leads to improvements in GPP_{yield} and SIF_{yield} (Fig 3). Nevertheless, after the assimilation there are still disagreements in SIF_{yield} vs GPP_{yield} relative to the measured quantities (Fig S8). For diurnal and synoptic cycles, the assimilation effectively acts to scale the magnitude of SIF, GPP and APAR (and related yields), but it does little to alter variability. Although data assimilation (i.e. calibrating model parameters) is critical to improving modelled SIF and GPP, this should be done in conjunction with improvements in the model formulation (as summarized in Section 5), otherwise the estimated model parameters can be sub-optimal to compensate for the lack of missing processes.

5. Conclusions/Recommendations

Our results reveal systematic biases across TBM-SIF models affecting leaf-to-canopy simulations of APAR, GPP, and SIF. This highlights key areas where observing strategies and model formulations can be improved:

- 1) Radiative transfer of incoming and absorbed PAR. The representation of incoming radiative transfer produces positive biases in APAR that leads to positive biases in GPP, both of which occur regardless of time of day. This is influenced by characterization of the canopy, leaf orientation and clumping, biochemical content, canopy layers, and leaf area, which dictates

the sunlit/shaded fractions of the canopy. Furthermore, the combination of high APAR bias in models and high uncertainty in observed APAR highlights a need for more accurate and representative *in situ* measurements of APAR within the FOV of SIF observations and footprint of eddy covariance data. We recommend further site-level investigation of observed and simulated canopy light absorption, emphasizing comparison of multi-layer and multi-leaf radiation schemes accounting for sunlit and shaded leaf area.

2) Water stress impacts on photosynthesis. The underlying photosynthetic models fail to simulate the magnitude of depression of observed GPP in the afternoon, regardless of how stomatal-conductance and water stress models and parameters are formulated. This likely results from the inability to account for afternoon water stress to properly restrict stomatal conductance and hence GPP and SIF. Additional effort is needed to characterize SIF and GPP sensitivity to increased atmospheric demand and/or reduced soil moisture across a range of managed and unmanaged systems. We also recommend more inclusion of stomatal optimization models (e.g., Eller et al., 2020) as optional parameterizations for TBMs, to better account for plant hydraulic functioning under water stress compared to the more widely used semi-empirical models.

3) Leaf Mechanism for Energy Partitioning. We provide evidence that many models fail to capture the correct reversible NPQ response to light saturation, leading to biases in SIF_{yield} during high light conditions and especially with increasing moisture limitation at the end of summer. Further investigation using models such as BETHY and CLM is needed to better characterize sensitivity of NPQ formulations to PFT and environmental conditions. We also emphasize a need for more simultaneous measurements of active and passive chlorophyll fluorescence to determine the temporal dynamics of competing pathways (PQ, NPQ) from a wider variety of plant species under ambient conditions and different levels of stress.

4) Radiative transfer of SIF. SIF is emitted from the leaf level and then is transferred to the top of canopy as a function of canopy structure (leaf geometry, canopy layers, leaf area, [sunlit/shaded fraction](#)). Despite high disagreement of SCOPE and BETHY with respect to the simulation of APAR and SIF magnitude, we recommend site level simulations using a similar

Deleted: (sunlit shaded fractions of leaf level)

framework where a radiative transfer model is run both offline and coupled to a terrestrial biosphere model for more detailed investigation of sensitivity to canopy characteristics.

5) Observation strategy. The PhotoSpec scan strategy enables direct measurement of SIF emission at leaf-to-canopy scale, but requires off-nadir view angles that lead to changing fractions of sunlit and shaded canopies throughout the day as a function of sun angle. Further work could be done using tower mounted instruments with a wider FOV that more accurately represent top of canopy emissions for comparison to model simulations, and to classify emissions from shaded vs sunlit canopies. More effort is also needed to better align models with observations, for example by leveraging three-dimensional capabilities in SCOPE (and other RTMs) to directly account for multiple observation angles.

6) Finally, we note that our focus on a water limited subalpine evergreen needleleaf forest represents a challenging case study for models and observations. In many cases, there is strong covariance between LAI, SIF, APAR and GPP in cropping systems (Dechant et al., 2020), but because this study site experiences little change in canopy structure and APAR throughout the season (Magney et al, 2019b), our study sought to provide more explicit insight into the models sensitivity to photosynthesis and fluorescence. As such, it is possible that we would see more convergence of results, and a reduction in confounding effects (e.g., decreased NPQ), in a well-watered high-LAI cropping system. We therefore recommend similar model-observation assessments across a wider range of biota and climate.

Data availability

All observational data (APAR, SIF, GPP, and relative SIF) are provided as hourly time series. The data can be found at <https://data.caltech.edu/records/1231>. The data are saved as a .csv file.

Author Contribution

NP, TM, and IB designed research. NP, TM, AN, BR, CB, FM, IB, YZ, BQ, MS, DB performed research; AN, BR, CB, FM, IB, YZ, BQ, MS, NM contributed model simulations; TM, DB, SP, PB, JS, KG, CF contributed observational data; NP, TM, AN, BR analyzed data; NP, TM, AN, BR, CB, IB, YZ, NM, DB, CF wrote paper.

967 **Competing Interests**

968 The authors declare that they have no conflict of interest.

969 **Acknowledgements**

970 The US-NR1 AmeriFlux site is supported by the U.S. DOE, Office of Science through the AmeriFlux
971 Management Project (AMP) at Lawrence Berkeley National Laboratory under Award Number
972 7094866. BMR was supported by the NASA CMS Project (award NNX16AP33G) and the US
973 Department of Energy's Office of Science, Terrestrial Ecosystem Science Program (awards DE-
974 SC0010624 and DE-SC0010625). CESM (CLM4.5 and CLM5.0) is sponsored by the National
975 Science Foundation and the U.S. Department of Energy. ORCHIDEE is supported by CNES-
976 TOSCA under the FluOR and ECOFLUO projects. ITB was supported by NASA contract
977 80NSSC18K1312. We would like to thank the W.M. Keck Institute for Space Studies and internal
978 funds from the Jet Propulsion Laboratory for support of the field measurements at Niwot Ridge
979 (<http://www.kiss.caltech.edu/study/photosynthesis/technology.html>). A portion of this research
980 was carried out at the Jet Propulsion Laboratory, California Institute of Technology, under
981 contract with NASA. This work was supported in part by the NASA Earth Science Division
982 MEaSUREs program (grant 17-MEASURES-0032) and ABoVE program (18-TE18-0062). Copyright
983 2020. All rights reserved.

984

985 **References**

- 986 Aasen, H., Van Wittenberghe, S., Medina, N. S., Damm, A., Goulas, Y., Wieneke, S., Hueni, A.,
 987 Malenovsky, Z., Alonso, L., Pacheco-Labrador, J., and Cendrero-Mateo, M.P.: Sun-induced
 988 chlorophyll fluorescence II: Review of passive measurement setups, protocols, and their
 989 application at the leaf to canopy level. *Remote Sensing*, 11(8), p.927, 2019.
- 990 Anav, A., Friedlingstein, P., Beer, C., Ciais, P., Harper, A., Jones, C., Murray-Tortarola, G., Papale,
 991 D., Parazoo, N.C., Peylin, P., and Piao, S.: Spatiotemporal patterns of terrestrial gross
 992 primary production: A review, *Reviews of Geophysics*, 53(3), 785-818,
 993 <https://doi.org/10.1002/2015RG000483>, 2015.
- 994 Albert, L. P., Keenan, T. F., Burns, S. P., Huxman, T. E., and Monson, R. K.: Climate controls over
 995 ecosystem metabolism: insights from a fifteen-year inductive artificial neural network
 996 synthesis for a subalpine forest, *Oecologia*, 184(1), 25–41.
 997 <https://doi.org/10.1007/s00442-017-3853-0>, 2017
- 998 Bacour, C., Maignan, F., MacBean, N., Porcar-Castell, A., Flexas, J., Frankenberg, C., Peylin, P.,
 999 Chevallier, F., Vuichard, N., and Bastrikov, V.: Improving estimates of Gross Primary
 1000 Productivity by assimilating solar-induced fluorescence satellite retrievals in a terrestrial
 1001 biosphere model using a process-based SIF model, *Journal of Geophysical Research:*
 1002 *Biogeosciences*, 124(11), 3281-3306, 2019.
- 1003 Baker, I.T., Prihodko, L., Denning, A.S., Goulden, M., Miller, S., and da Rocha, H.: Seasonal
 1004 Drought Stress in the Amazon: Reconciling Models and Observations, *J.Geophys. Res.*, 113,
 1005 G00B01, doi:10.1029/2007JG000644, 2008.
- 1006 Baker, I.T., A.S. Denning, N. Hanan, L. Prihodko, P.-L. Vidale, K. Davis and P. Bakwin: Simulated
 1007 and observed fluxes of sensible and latent heat and CO2 at the WLEF-TV Tower using
 1008 SiB2.5, *Glob. Change Biol.*, 9, 1262-1277, 2003.
- 1009 Ball, J. T., Woodrow, I. E., and Berry, J. A.: A model predicting stomatal conductance and its
 1010 contribution to the control of photosynthesis under different environmental
 1011 conditions, *Progress in photosynthesis research*, Springer, Dordrecht, 221-224, 1987.
- 1012 Burns, S. P., Blanken, P. D., Turnipseed, A. A., Hu, J., and Monson, R. K.: The influence of warm-
 1013 season precipitation on the diel cycle of the surface energy balance and carbon dioxide at
 1014 a Colorado subalpine forest site, *Biogeosciences*, 12, 7349–7377, 2015.
- 1015 Burns, S. P., Swenson, S. C., Wieder, W. R., Lawrence, D. M., Bonan, G. B., Knowles, J. F., and
 1016 Blanken, P. D.: A comparison of the diel cycle of modeled and measured latent heat flux
 1017 during the warm season in a Colorado subalpine forest, *Journal of Advances in Modeling*
 1018 *Earth Systems*, 10, 617–651, 2018.

1019 Chen, J. M., Liu, J., Cihlar, J., and Goulden, M. L.: Daily canopy photosynthesis model through
 1020 temporal and spatial scaling for remote sensing applications, *Ecological Modelling*, 124(2–
 1021 3), 99–119, 1999.

1022 Demmig-Adams, B., Cohu, C. M., Muller, O., and Adams, W. W.: Modulation of photosynthetic
 1023 energy conversion efficiency in nature: from seconds to seasons, *Photosynthesis Research*,
 1024 113(1–3), 75–88. <https://doi.org/10.1007/s11120-012-9761-6>, 2012.

1025 Dechant, B., Ryu, Y., Badgley, G., Zeng, Y., Berry, J.A., Zhang, Y., Goulas, Y., Li, Z., Zhang, Q.,
 1026 Kang, M., Li, J., Moya, I.: Canopy structure explains the relationship between
 1027 photosynthesis and sun-induced chlorophyll fluorescence in crops, *Remote Sensing of*
 1028 *Environment*, 241, 111733, 2020.

1029 Dufresne, J.-L., Foujols, M.-A., Denvil, S., Caubel, A., Marti, O., Aumont, O., Balkanski, Y., Bekki,
 1030 S., Bellenger, H., Benshila, R., and Bony, S.: Climate change projections using the IPSL-CM5
 1031 Earth System Model: from CMIP3 to CMIP5, *Climate Dynamics*, 40(9–10), 2123–2165,
 1032 2013.

1033 Eller, Cleiton B., Rowland, L., Mencuccini, M., Rosas, T., Williams, K., Harper, A., Medlyn, B. E.,
 1034 Wagner, Y., Klein, T., Teodoro, G.S. and Oliveira, R.S.: Stomatal optimisation based on
 1035 xylem hydraulics (SOX) improves land surface model simulation of vegetation responses to
 1036 climate, *New Phytologist*, 2020.

1037 Flexas, J., Escalona, J. M., Evain, S., Gulías, J., Moya, I., Osmond, C. B., and Medrano, H.: Steady-
 1038 state chlorophyll fluorescence (Fs) measurements as a tool to follow variations of net CO₂
 1039 assimilation and stomatal conductance during water-stress in C₃ plants. *Physiologia*
 1040 *Plantarum*, 114(2), 231–240. <https://doi.org/10.1034/j.1399-3054.2002.1140209.x>, 2002.

1041 Friedlingstein, P., Meinshausen, M., Arora, V. K., Jones, C. D., Anav, A., Liddicoat, S. K., and
 1042 Knutti, R.: Uncertainties in CMIP5 climate projections due to carbon cycle feedbacks,
 1043 *Journal of Climate*, 27(2), 511–526, 2014.

1044 Galmés, J., Flexas, J., Savé, R., and Medrano, H.: Water relations and stomatal characteristics of
 1045 Mediterranean plants with different growth forms and leaf habits: responses to water
 1046 stress and recovery, *Plant and Soil*, 290(1–2), 139–155, 2007.

1047 Gastellu-Etchegorry, J. P., Malenovsky, Z., Duran Gomez, N., Meynier, J., Lauret, N., Yin, T., Qi,
 1048 J., Guilleux, J., Chavanon, E., Cook, B., Morton, D.: Simulation of chlorophyll fluorescence
 1049 for sun- and shade-adapted leaves of 3D canopies with the DART model, *International*
 1050 *Geoscience and Remote Sensing Symposium (IGARSS)*, 2018-July, 5995–5998.
 1051 <https://doi.org/10.1109/IGARSS.2018.8517576>, 2018.

1052 Grossmann, K., Frankenberg, C., Magney, T. S., Hurlock, S. C., Seibt, U., and Stutz, J.: PhotoSpec:
 1053 A new instrument to measure spatially distributed red and far-red Solar-Induced
 1054 Chlorophyll Fluorescence, *Remote Sensing of Environment*, 216, 311–327.
 1055 <https://doi.org/10.1016/j.rse.2018.07.002>, 2018.

1056 Gu, L., Han, J., Wood, J. D., Chang, C. Y., and Sun, Y.: Sun-induced Chl fluorescence and its
 1057 importance for biophysical modeling of photosynthesis based on light reactions, *New*
 1058 *Phytologist*, nph.15796. <https://doi.org/10.1111/nph.15796>, 2019.

1059 Gu, L., Wood, J. D., Chang, C. Y. Y., Sun, Y., and Riggs, J. S.: Advancing Terrestrial Ecosystem
 1060 Science With a Novel Automated Measurement System for Sun-Induced Chlorophyll
 1061 Fluorescence for Integration With Eddy Covariance Flux Networks, *Journal of Geophysical*
 1062 *Research: Biogeosciences*, 124(1), 127–146. <https://doi.org/10.1029/2018JG004742>, 2019.

1063 Haynes, K., Baker, I. T., Denning, S., Stöckli, R., Schaefer, K., Lokupitiya, E. Y., and Haynes, J. M.:
 1064 Representing grasslands using dynamic prognostic phenology based on biological growth
 1065 stages: 1. Implementation in the Simple Biosphere Model (SiB4), *Journal of Advances in*
 1066 *Modeling Earth Systems*, 11. <https://doi.org/10.1029/2018MS001540>, 2019a.

1067 Haynes, K. D., Baker, I. T., Denning, A. S., Wolf, S., Wohlfahrt, G., Kiely, G., Minaya, R. C., and
 1068 Haynes, J. M.: Representing grasslands using dynamic prognostic phenology based on
 1069 biological growth stages: 2. Carbon cycling, *Journal of Advances in Modeling Earth*
 1070 *Systems*, 11. <https://doi.org/10.1029/2018MS001541>, 2019b.

1071 Julitta, T., Burkart, A., Colombo, R., Rossini, M., Schickling, A., Migliavacca, M., Cogliati, S.,
 1072 Wutzler, T., Rascher, U.: Accurate measurements of fluorescence in the O2A and O2B band
 1073 using the FloX spectroscopy system - results and prospects. In: *Proc. Potsdam GHG Flux*
 1074 *Workshop: From Photosystems to Ecosystems*, 24–26 October 2017, Potsdam, Germany.
 1075 <https://www.potsdam-flux-workshop.eu/>, 2017

1076 Kaminski, T., Knorr, W., Schürmann, G., Scholze, M., Rayner, P. J., Zaehle, S., Blessing, S., Dorigo,
 1077 W., Gayler, V., Giering, R., and Gobron, N.: The BETHY/JSBACH carbon cycle data
 1078 assimilation system: Experiences and challenges, *Journal of Geophysical Research:*
 1079 *Biogeosciences*, 118(4), 1414–1426, 2013.

1080 Kennedy, D., Swenson, S., Oleson, K. W., Lawrence, D. M., Fisher, R., Lola da Costa, A. C., and
 1081 Gentine, P.: Implementing plant hydraulics in the community land model, version
 1082 5, *Journal of Advances in Modeling Earth Systems*, 11(2), 485–513, 2019.

1083 Koffi, E. N., Rayner, P. J., Scholze, M., and Beer, C.: Atmospheric constraints on gross primary
 1084 productivity and net ecosystem productivity: Results from a carbon-cycle data assimilation
 1085 system, *Global Biogeochemical Cycles*, 26(1), <https://doi.org/10.1029/2010GB003900>,
 1086 2012.

1087 Koffi, E. N., Rayner, P. J., Norton, A. J., Frankenberg, C., and Scholze, M.: Investigating the
 1088 usefulness of satellite-derived fluorescence data in inferring gross primary productivity
 1089 within the carbon cycle data assimilation system, *Biogeosciences*, 12(13), 4067–4084,
 1090 2015.

1091 Krinner, G., Viovy, N., de Noblet-Ducoudré, N., Ogée, J., Polcher, J., Friedlingstein, P., Ciais, P.,
1092 Sitch, S., and Prentice, I. C.: A dynamic global vegetation model for studies of the coupled
1093 atmosphere-biosphere system, *Global Biogeochemical Cycles*, 19(1), 2005.

1094 Lee, J.-E., Berry, J. A., van der Tol, C., Yang, X., Guanter, L., Damm, A., Baker, I., and
1095 Frankenberg, C.: Simulations of chlorophyll fluorescence incorporated into the Community
1096 Land Model version 4, *Global change biology*, 21 (9), 3469-3477, 2015.

1097 Leuning R.: A critical appraisal of a combined stomatal-photosynthesis model for
1098 C₃ plants, *Plant Cell Environ*, **18**: 339–357, 1995.

1099 Li, Z., Zhang, Q., Li, J., Yang, X., Wu, Y., Zhang, Z., Wang, S., Wang, H., and Zhang, Y.: Solar-
1100 induced chlorophyll fluorescence and its link to canopy photosynthesis in maize from
1101 continuous ground measurements, *Remote Sensing of Environment*, 236, 111420, 2020.

1102 Liu, J., Chen, J. M., and Cihlar, J.: Mapping evapotranspiration based on remote sensing: An
1103 application to Canada's landmass, *Water Resources Research*, 39(7), 2003.

1104 Liu, W., Atherton, J., Möttus, M., Gastellu-Etchegorry, J. P., Malenovsky, Z., Raunonen, P., et
1105 al.: Simulating solar-induced chlorophyll fluorescence in a boreal forest stand
1106 reconstructed from terrestrial laser scanning measurements, *Remote Sensing of*
1107 *Environment*, (July 2018), 111274, <https://doi.org/10.1016/j.rse.2019.111274>, 2019.

1108 Medlyn, B.E., Duursma, R.A., Eamus, D., Ellsworth, D.S., Prentice, I.C., Barton, C.V.M., Crous, K.Y.,
1109 De Angelis, P., Freeman, M., and Wingate, L.: Reconciling the optimal and empirical
1110 approaches to modelling stomatal conductance, *Global Change Biology*, 17: 2134–2144.
1111 doi:10.1111/j.1365-2486.2010.02375.x, 2011.

1112 Magney, T. S., Frankenberg, C., Fisher, J. B., Sun, Y., North, G. B., and Davis, T. S.: Connecting
1113 active to passive fluorescence with photosynthesis : a method for evaluating remote
1114 sensing measurements of Chl fluorescence, *New Phytologist*, 215(4), 1594-1608,
1115 <https://doi.org/10.1111/nph.14662>, 2017.

1116 Magney, T. S., Frankenberg, C., Köhler, P., North, G., Davis, T. S., Dold, C., Dutta, D., Fisher, J. B.,
1117 Grossmann, K., Harrington, A., Hatfield, J.: Disentangling Changes in the Spectral Shape of
1118 Chlorophyll Fluorescence: Implications for Remote Sensing of Photosynthesis, *Journal of*
1119 *Geophysical Research: Biogeosciences*, 124(6), 1491-1507,
1120 <https://doi.org/10.1029/2019JG005029>, 2019a.

1121 Magney, T. S., Bowling, D. R., Logan, B., Grossmann, K., Stutz, J., and Blanken, P.: Mechanistic
1122 evidence for tracking the seasonality of photosynthesis with solar-induced fluorescence,
1123 *Proceedings of the National Academy of Sciences*, 116 (24), 11640-11645,
1124 <https://doi.org/10.1073/pnas.1900278116>, 2019b.

1125 Magney, T., Frankenberg, C., Grossmann, K., Bowling, D., Logan, B., Burns, S., and Stutz,
 1126 J.: Canopy and needle scale fluorescence data from Niwot Ridge, Colorado 2017-
 1127 2018 (Version 1.1) [Data set]. CaltechDATA. <https://doi.org/10.22002/d1.1231>. 2019c.

1128 Miguez, F., Fernández-Marin, B., Becerril, J. M., and Garcia-Plazaola, J. I.: Activation of
 1129 photoprotective winter photoinhibition in plants from different environments: a literature
 1130 compilation and meta-analysis, *Physiologia Plantarum*, 155(4), 414–423, 2015.

1131 Mohammed, G. H., Colombo, R., Middleton, E. M., Rascher, U., van der Tol, C., Nedbal, L.,
 1132 Goulán, Y., Perez-Priego, O., Damm, A., Meroni, M. and Joiner, J.: Remote sensing of solar-
 1133 induced chlorophyll fluorescence (SIF) in vegetation: 50 years of progress, *Remote Sensing*
 1134 *of Environment*, 231, 111177, <https://doi.org/10.1016/j.rse.2019.04.03>, 2019.

1135 Monteith, J. L.: Solar Radiation and Productivity in Tropical Ecosystems, *J. Appl. Ecol.*, 9, 747–
 1136 766, <https://doi.org/10.2307/2401901>, 1972.

1137 Norton, A. J., Rayner, P. J., Koffi, E. N., and Scholze, M.: Assimilating solar-induced chlorophyll
 1138 fluorescence into the terrestrial biosphere model BETHY-SCOPE v1. 0: model description
 1139 and information content, *Geoscientific Model Development*, 11(4), 1517–1536, 2018.

1140 Norton, A. J., Rayner, P. J., Koffi, E. N., Scholze, M., Silver, J. D., and Wan, Y.-P.: Estimating global
 1141 gross primary productivity using chlorophyll fluorescence and a data assimilation system
 1142 with the BETHY-SCOPE model, *Biogeosciences*, 16(15), 3069–3093, 2019.

1143 Porcar-Castell, A.: A high-resolution portrait of the annual dynamics of photochemical and non-
 1144 photochemical quenching in needles of *Pinus sylvestris*, *Physiologia Plantarum*, 143(2),
 1145 139–153, <https://doi.org/10.1111/j.1399-3054.2011.01488.x>, 2011.

1146 Qiu, B., Chen, J. M., Ju, W., Zhang, Q., and Zhang, Y.: Simulating emission and scattering of
 1147 solar-induced chlorophyll fluorescence at far-red band in global vegetation with different
 1148 canopy structures, *Remote Sensing of Environment*, 111373, 2019.

1149 Raczka, B., Duarte, H. F., Koven, C. D., Ricciuto, D., Thornton, P. E., Lin, J. C., & Bowling, D. R.: An
 1150 observational constraint on stomatal function in forests: evaluating coupled carbon and
 1151 water vapor exchange with carbon isotopes in the Community Land Model (CLM4.
 1152 5), *Biogeosciences*, 13(18), 5183–5204, 2016.

1153 Raczka, B., Porcar-Castell, A., Magney, T., Lee, J. E., Köhler, P., Frankenberg, C., Grossman, K.,
 1154 Logan, B.A., Stutz, J., Blanken, P. D., Burns, S. P., Duarte, H., Yang, X., Lin, J. C., and Bowling,
 1155 D. R.: Sustained nonphotochemical quenching shapes the seasonal pattern of solar-
 1156 induced fluorescence at a high-elevation evergreen forest, *Journal of Geophysical*
 1157 *Research: Biogeosciences*, 124, 2005–2020, <https://doi.org/10.1029/2018JG004883>, 2019.

1158 Rayner, P. J., Scholze, M., Knorr, W., Kaminski, T., Giering, R., and Widmann, H.: Two decades of
 1159 terrestrial carbon fluxes from a carbon cycle data assimilation system (CCDAS), *Global*
 1160 *Biogeochemical Cycles*, 19(2), 2005.

1161 Schreiber, U., Schliwa, U., and Bilger, W.: Continuous recording of photochemical and non-
 1162 photochemical chlorophyll fluorescence quenching with a new type of modulation
 1163 fluorometer, *Photosynthesis Research*, 10, 51–62, 1986.

1164 Sellers, P. J., Randall, D. A., Collatz, G. J., Berry, J. A., Field, C. B., Dazlich, D. A., Zhang, C., Collelo,
 1165 G. D., and Bounoua, L.: A revised land surface parameterization (SiB2) for atmospheric
 1166 GCMs. Part I: Model formulation, *Journal of Climate*, 9(4), 676–70, 1996.

1167 Shan, N., Ju, W., Migliavacca, M., Martini, D., Guanter, L., Chen, J., Goulas, Y., Zhang, Y.:
 1168 Modeling canopy conductance and transpiration from solar-induced chlorophyll
 1169 fluorescence. *Agricultural and Forest Meteorology*, 268, 189–201, 2019.

1170 Svishnikov, D., Ensminger, I., Ivanov, A. G., Campbell, D., Lloyd, J., Funk, C., Huner, N. P. A.,
 1171 Oquist, G.: Excitation energy partitioning and quenching during cold acclimation in Scots
 1172 pine. *Tree Physiology*, 26(3), 325–336, 2006.

1173 Van Der Tol, C., Berry, J. A., Campbell, P. K. E., and Rascher, U.: Models of fluorescence and
 1174 photosynthesis for interpreting measurements of solar-induced chlorophyll fluorescence,
 1175 *Journal of Geophysical Research: Biogeosciences*, 119(12), 2312–2327.
 1176 <https://doi.org/10.1002/2014JG002713>, 2014.

1177 Wohlfahrt, G., Gerdel, K., Migliavacca, M., Rotenberg, E., Tatarinov, F., Müller, J., Hammerle,
 1178 A., Julitta, T., Spielmann, F.M., Yakir, D.: Sun-induced fluorescence and gross primary
 1179 productivity during a heat wave. *Sci. Rep.*, 8, 1–9, 2018.

1180 Yang, P., and van der Tol, C.: Linking canopy scattering of far-red sun-induced chlorophyll
 1181 fluorescence with reflectance, *Remote Sensing of Environment*, 209(May), 456–467.
 1182 <https://doi.org/10.1016/j.rse.2018.02.029>, 2018.

1183 Yin, X., and Struik, P. C.: C3 and C4 photosynthesis models: an overview from the perspective of
 1184 crop modelling, *NJAS-Wageningen Journal of Life Sciences*, 57(1), 27–38, 2009.

1185 Zhang, Y., Guanter, L., Berry, J. A., van der Tol, C., Yang, X., Tang, J., and Zhang, F.: Model-based
 1186 analysis of the relationship between sun-induced chlorophyll fluorescence and gross
 1187 primary production for remote sensing applications, *Remote Sensing of Environment*, 187,
 1188 145–155, 2016.

1189 Zhang, Q., Zhang, X., Li, Z., Wu, Y., and Zhang, Y.: Comparison of Bi-Hemispherical and
 1190 Hemispherical-Conical Configurations for In Situ Measurements of Solar-Induced
 1191 Chlorophyll Fluorescence, *Remote Sensing*, 11, 2642, 2019.

1192

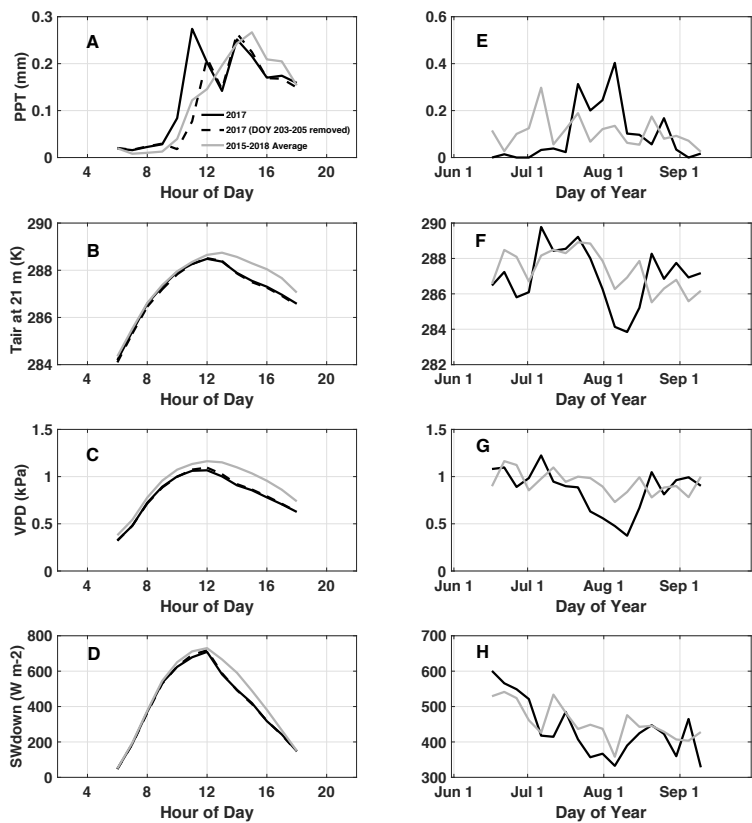
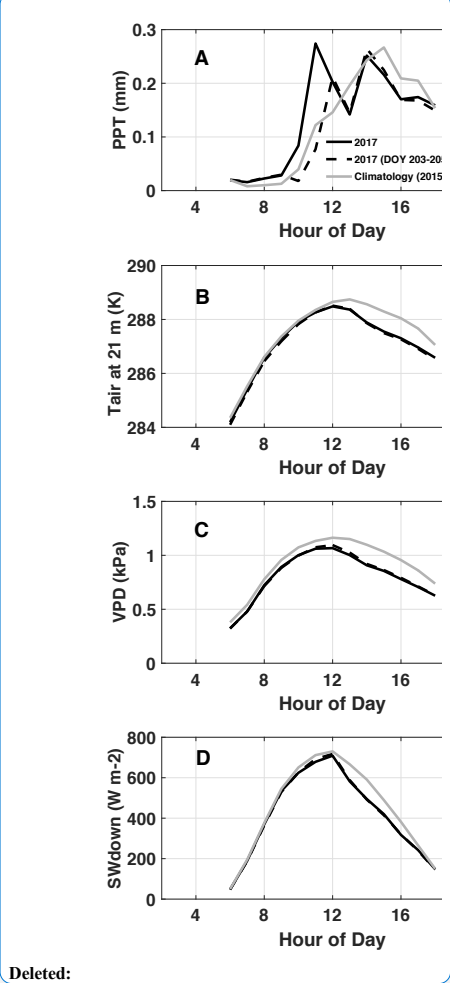


Figure 1. Observed diurnal (A-D) and synoptic (E-H) precipitation (PPT), air temperature at 21 m (Tair), vapor pressure deficit (VPD), and downwelling shortwave (SWdown). Diurnal cycles are averaged over July-August, 2017. Synoptic cycles are plotted as 5-day averages from June 15 – Sep 15. Data from 2017 is shown in black and climatology (2015-2018) in grey. Typically, peak rainfall occurs in the afternoon at this site (A). A substantial rain event which occurred from DOY 203-205 is removed from the 2017 average to show the impact on diurnal variability and to demonstrate the dominance of the afternoon monsoon upon diurnal precipitation in summer.



Deleted:

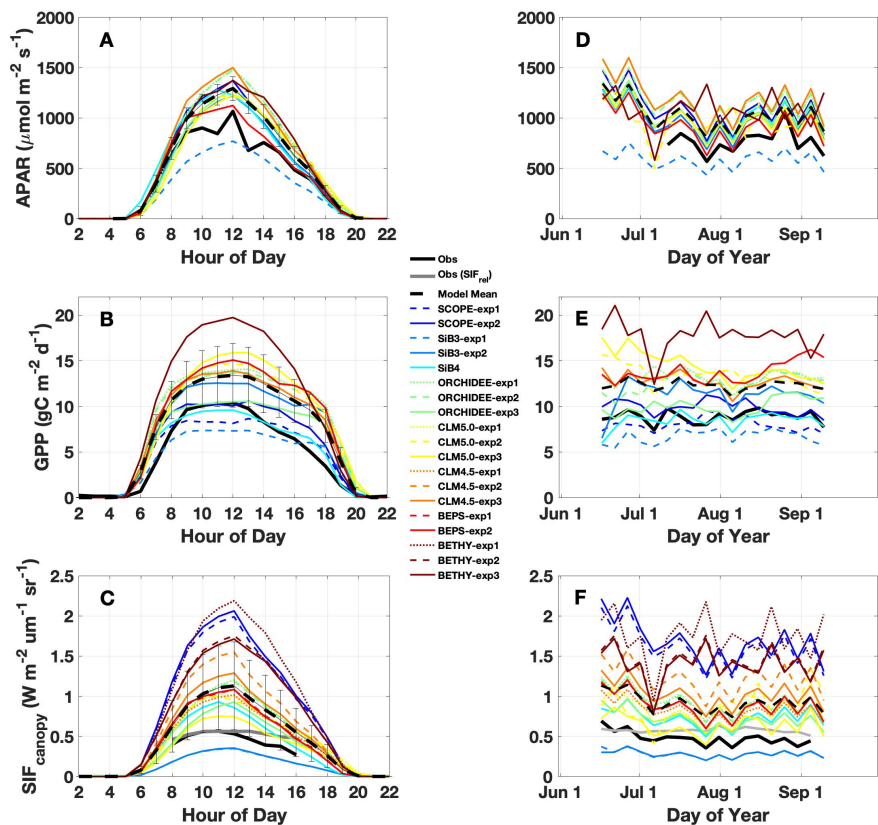


Figure 2. Observed and simulated diurnal and synoptic cycles of APAR, GPP and SIF. Diurnal cycles (A-C) are averaged over July-August, 2017. Synoptic cycles (D-F) are plotted as 5-day averages from June 15 – Sep 15. Observations are shown in black, with relative SIF (SIF_{canopy} / far red reflected radiance) included in (C, F) in grey. The across model average (dashed black) represents the average of "best-case" model scenarios (solid lines; SCOPE-exp2, SiB3-exp2, SiB4, ORCHIDEE-exp3, CLM5.0-exp3, CLM4.5-exp3, BEPS-exp2, BETHY-exp3) with uncertainty bars indicating the across model 1 sigma uncertainty.

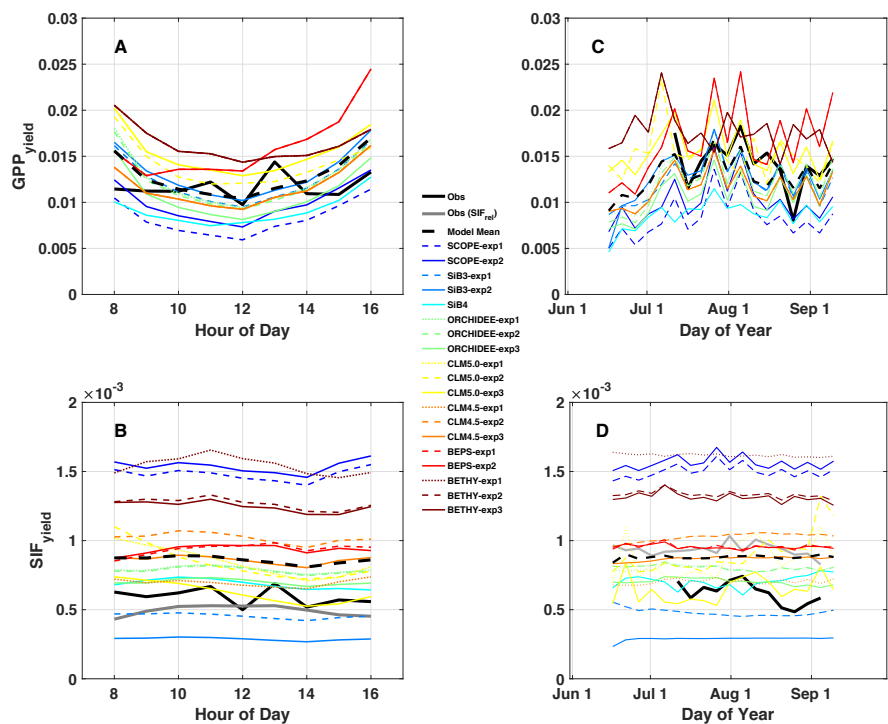


Figure 3. Same as Figure 2 except for SIF_{yield} and GPP_{yield}. Here, SIF_{yield} = SIF_{canopy} / APAR, and GPP_{yield} = GPP / APAR. As with Figure 2, the left column shows the mean diurnal cycle, and the right column shows a time series of 5-day averages.

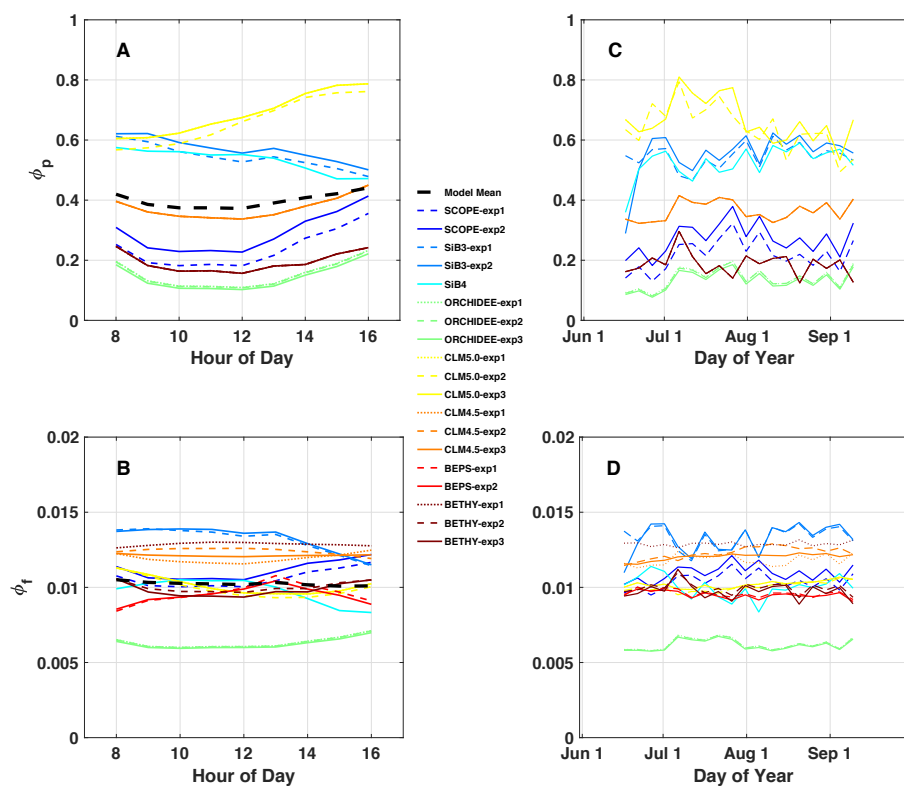


Figure 4. Same as Figure 2, except for quantum yield of fluorescence (ϕ_F) and photochemistry (ϕ_P).

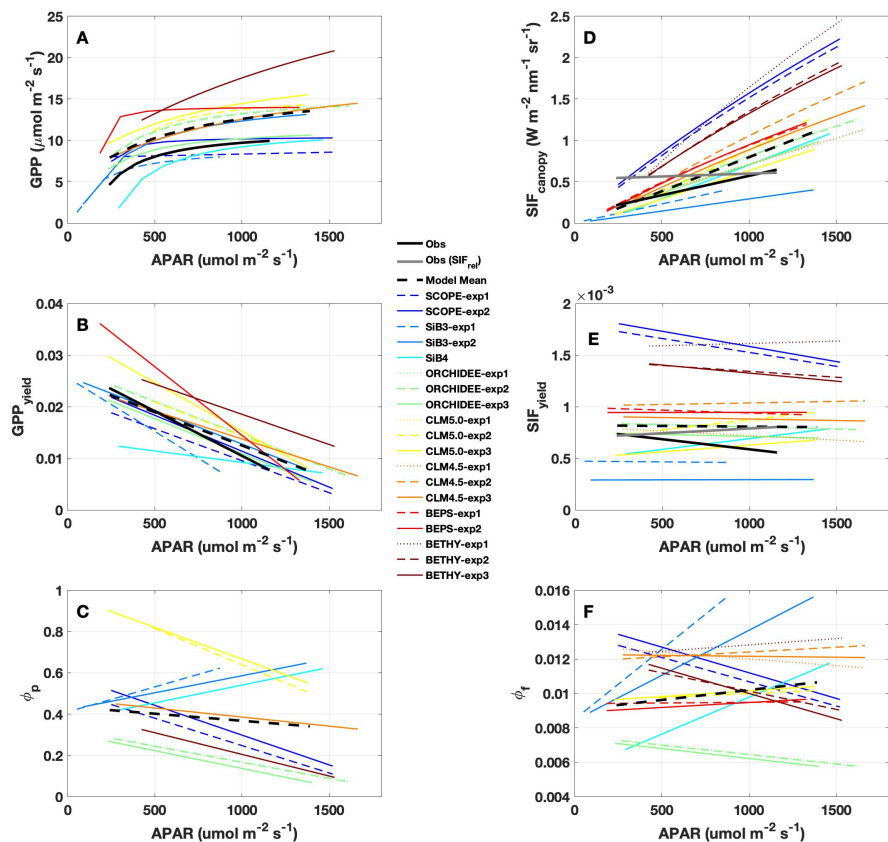


Figure 5. Observed and predicted change in GPP, SIF, and yields with APAR. Regression lines are shown for (A) GPP, (B) GPP_{yield} , (C) photochemical quantum yield (ϕ_p), (D) SIF_{canopy} , (E) SIF_{yield} , (F) fluorescence quantum yield (ϕ_f), as a function of APAR, using daily mean (8 am – 4 pm local) values over the period July-August 2017. Observations are shown in solid black, individual models and experiments in color, the across model average in dashed black. Relative SIF is shown in grey in (D) and (E).

1232 **Tables**

Model (citation)	Model Experiments	Stomatal Conductance	Canopy Type / Radiation	Stress	Vcmax	LAI	k _N	Leaf-to-Canopy Scaling	Parameter Optimization
SCOPE v1.73 (van der Tol, 2014)	SCOPE-exp1	Ball-Berry-Woodrow	Multi-layer Sunlit/Shaded = Yes F _{par} /APAR = semi-analytical canopy radiative model (based on SNL)	Ta stress	Prescribed (30)	Prescribed (4.0 m ² m ⁻²)	Adapted to drought stressed Mediterranean species including high temperature correction (Tol et al., 2014; Flexas et al., 2002)	60 layer 1D radiative transfer	Hand-tuned to NR1 (Raczka et al., 2016)
	SCOPE-exp2				Seasonally calibrated to NR1				
BETHY (Norton et al., 2019)	BETHY-exp1	Ball-Berry-Woodrow	Same as SCOPE	Ta stress	Prior is a function of Ta	Prescribed (4.0 m ² m ⁻²)	Adapted to unstressed cotton species (Tol et al., 2014)	SCOPE radiative transfer. f(Ta, APAR, structure, leaf composition) via dependence of photosynthetic rate on Φ	Default
	BETHY-exp2						Adapted to drought stressed Mediterranean species including high temperature correction (Tol et al., 2014; Flexas et al., 2002)		
	BETHY-exp3						Adapted to drought stressed Mediterranean species (Flexas et al., 2002)		
ORCHIDEE (Bacour et al., 2019)	ORCHIDEE-exp1	Yin-Struik	Big Leaf Sunlit/Shaded = No APAR = Beer-Lambert law depending on LAI and extinction factor = 0.5	Ta stress	f (leaf age, CO ₂ , Ta, water stress)	Prognostic	Adapted to needleleaf species (Porcar-Castell et al., 2011) and unstressed Mediterranean species (Flexas, 2002), with added dependence on PAR, temperature, and Φ	Parametric representation of SCOPE (v1.61) to emulate radiative transfer within canopy for PS/II.	Default
	ORCHIDEE-exp2								
	ORCHIDEE-exp3								
BEP5 (Qiu et al., 2019)	BEP5-exp1	Leuning	Two Leaf Sunlit/Shaded = Yes F _{par} = semi-analytical canopy radiative transfer	Soil water stress factor (ratio of measured soil available water to maximum plant available water)	Prescribed	Prescribed (4.0 m ² m ⁻²)	Adapted to water stressed Mediterranean species (Galmes et al., 2007)	Parametric representation of radiative transfer physics to account for canopy scattering effects	Default
	BEP5-exp2						Adapted to drought stressed Mediterranean species including high temperature correction (Tol et al., 2014; Flexas et al., 2002)		
CLM4.5 (Raczka et al., 2019)	CLM4.5-exp1	Ball-Berry-Woodrow	Two Big Leaf Sunlit/Shaded = Yes	Ta(Vcmax); soil moisture stress uses Brian parameterization (function of column rooting profile and soil water potential)	Prescribed (calibrated against observed GPP at NR1)	Prescribed (4.0 m ² m ⁻²)	Adapted to water stressed Mediterranean species (Galmes et al., 2007)	k _{veg} = f(Vcmax, SZA), calibrated to offline SCOPE runs using prescribed canopy characteristics at NR1	Hand-tuned to NR1 (Raczka et al., 2016)
	CLM4.5-exp2						Adapted to needleleaf species (Porcar-Castell et al., 2011); Accounts for sustained NPQ (k _N) separately from reversible NPQ (k _R). k _N is calibrated to NR1 Tair. k _N is fixed in time		
	CLM4.5-exp3						same as Exp 2, but k _N is seasonal		
CLM5.0 (unpublished)	CLM5.0-exp1	Medlyn	Two Big Leaf Sunlit/Shaded = Yes	Plant hydraulic water stress (Sperry and Love, 2015; Lawrence et al., 2015) accounting for water demand and supply	f (soil moisture, nitrogen), calibrated to NR1	Prescribed (4.0 m ² m ⁻²)	Adapted to water stressed Mediterranean species (Galmes et al., 2007)	k _{veg} = f(Vcmax), calibrated to offline SCOPE runs from Lee et al. (2015)	Default
	CLM5.0-exp2							k _{veg} = f(Vcmax, SZA), calibrated to offline SCOPE runs w/ prescribed canopy characteristics at NR1	
	CLM5.0-exp3							Escape ratio (f _{esc}), derived from Nlirv and IPAR (Zeng et al., 2019)	
SIB3 (Baker et al., 2003, 2008) SIB4 (Haynes et al., 2019a,b)	SIB3-exp1	Ball-Berry-Woodrow	Big Leaf Sunlit/Shaded = No	Downregulation by VPD, Ta, and soil moisture	f (soil moisture)	Prescribed (MCD10)	Adapted to drought stressed species (Tol et al., 2014)	k _{veg} = f(Vcmax), calibrated to offline SCOPE runs from Lee et al. (2015)	Default
	SIB3-exp2					Prescribed (4.0 m ² m ⁻²)			
	SIB4					Prognostic			

1233

1234 **Table 1.** Summary of TBM-SIF models and within model experiments illustrating model
1235 components that may have led to differences in modeled SIF., These include a representation of
1236 stomatal-conductance (column 3), canopy absorption of incoming radiation (column 4), limiting
1237 factors for photosynthesis (Stress, V_{cmax}, LAI; columns 5-7) and SIF (k_N; column 8), leaf-to-canopy
1238 scaling of SIF (column 9), and parameter optimization (column 10). The underlined model
1239 experiment was used for model intercomparison .

1240

1241

1242